Title: Plasma cells in human pancreatic ductal adenocarcinoma secrete antibodies to self-antigens

Authors: Min Yao[1]†, Jonathan Preall[1], Johannes Yeh[1], Darryl Pappin[1], Paolo Cifani[1], Yixin Zhao[1], Sophia Shen[2], Philip Moresco[1,3,4], Brian He[1], Hardik Patel[1], Amber Habowski [1], Daniel A. King[5], Kara Raphael[5], Arvind Rishi[5], Divyesh Sejpal[5]‡, Matthew Weiss[5], David Tuveson[1], Douglas Fearon[1,6*]

Affiliations:

[1]Cold Spring Harbor Laboratory, Cold Spring Harbor, NY 11724.

[2]Cold Spring Harbor High School, Cold Spring Harbor, NY 11724.

[3]Graduate Program in Genetics, Stony Brook University, Stony Brook, NY 11794.

[4]Medical Scientist Training Program, Stony Brook University Renaissance School of Medicine, Stony Brook University, Stony Brook, NY 11794.

[5]North Shore University Hospital, Manhasset, NY 11030.

[6]Weill Cornell Medicine, New York, NY 10065.

*Corresponding author. Email: dfearon@cshl.edu

†Present addresses: Tri-Institutional Therapeutics Discovery Institute, New York, NY 10021.

‡ Present addresses: Digestive Disease Institute, CommonSpirit Health Southwest Division and Dignity Health Medical Group, Phoenix, NY 85012.

One Sentence Summary: We have identified that plasma cells in human pancreatic ductal adenocarcinoma prominently secrete antibodies recognizing intracellular unmutated self-antigens.

Abstract:

Intratumoral B cell responses are associated with more favorable clinical outcomes in human pancreatic ductal adenocarcinoma (PDAC). However, the antigens driving these B cell responses are largely unknown. We sought to discover these antigens by using single-cell RNA sequencing (scRNA-Seq) and immunoglobulin (Ig) sequencing of tumor-infiltrating immune cells from seven primary PDAC samples. We identified activated T and B cell responses and evidence of germinal center reactions. Ig sequencing identified plasma cell (PC) clones expressing isotype-switched and hyper-mutated Igs, suggesting the occurrence of T cell-dependent B cell responses. We assessed the reactivity of 41 recombinant antibodies that represented the products of 235 PCs and 12 B cells toward multiple cell lines and PDAC tissues, and observed frequent staining of intracellular self-antigens. Three of these antigens were identified: the filamentous actin (F-actin), the nucleic protein, RUVBL2, and the mitochondrial protein, HSPD1. Antibody titers to F-actin and HSPD1 were elevated in the plasma of PDAC patients, and also detectable in healthy donors. Thus, PCs in PDAC produce auto-antibodies reacting with intracellular self-antigens, which may result from promotion of pre-existing, autoreactive B cell responses. These observations indicate that the chronic inflammatory microenvironment of PDAC can support the adaptive immune response.

56 **Main Text:**

57 **INTRODUCTION**

58 Microsatellite-stable PDACs do not respond to immunotherapy, have few T cells in cancer cell nests, and
59 have been thought to minimally stimulate the adaptive immune system (*1*). Recently, however, it has been
60 observed that PDAC patients whose tumors contained tertiary lymphoid structures (TLS) with germinal
61 centers, memory B cells, and memory CD4+ T cells had improved long-term survival (*2-4*), suggesting
62 the occurrence of clinically relevant, ongoing anti-PDAC immune responses. The possibility of these
63 immune responses is supported by a study involving patients with PDAC and colorectal cancer in which
64 one-week continuous administration of an inhibitor to the chemokine receptor, CXCR4, revealed on-
65 going anti-tumor immune responses (*5*).

66 The antigens driving these intratumoral immune reactions in human PDAC are unknown. Although
67 PDAC has a low mutational frequency compared to other cancers (*1*), attention has been directed to T cell
68 clones from PDAC patients with specificity to neoantigens arising from mutations that predicted cross-
69 reactive microbial epitopes (*6*). The intratumoral immune response may also be directed towards
70 germline-encoded antigens, a concept that has been supported by the finding that immunization of mice
71 with induced pluripotent stem cells confers protection against several tumor models (*7, 8*). Thus, defining
72 the range of antigens that are driving the intratumoral immune response in PDAC may expand our
73 knowledge of the interaction between this cancer and the immune system.

74 B cell activation is triggered by antigen interaction with membrane immunoglobulin (Ig). This
75 interaction may lead to B cell activation, antigen-presentation to CD4 T cells, and the formation of
76 germinal center reactions. The latter will lead to B cell clonal expansion, heavy (H) chain isotype
77 switching, H chain and light (L) chain variable region somatic hypermutation (SHM), and ultimately
78 differentiation into antibody-secreting PCs. Therefore, antibodies derived from activated B cell responses
79 may help identify those antigens that are driving intratumoral immune responses. In the current report, we
80 have used scRNA-Seq of PCs and B cells from primary PDAC specimens to identify their paired H and L
81 chains which enabled screening of antibody reactivity.

82 **RESULTS**

83 **Identification of B and T cell responses by scRNA-Seq in human PDAC**

84 We performed scRNA-Seq of CD45+ immune cells from seven untreated primary PDAC samples,
85 including four microsatellite-stable surgically resected tumors and three fine-needle aspiration (FNA)
86 biopsies (Table S1). scRNA-Seq identified a total of 26,702 immune cells and 327 non-immune cells. The
87 major immune cells included T cells (66%), myeloid cells (19%), PCs (7.4%) and B cells (3.6%), with T
88 and myeloid cells being the most frequent cell types in each sample (Fig. 1A-B and Fig. S1A). In the
89 *CD8+* T cells, features of T cell activation were prominent, as evidenced by frequent expression of the
90 effector genes, *PRF1* (46% of CD8 T cells) and *GZMB* (31%), as well as the cytokines, *IFNG* (13%) and
91 *TNF* (11%). Subsets of *CD8+* T cells also expressed the inhibitory receptors, *PD-1* (14%) and *CTLA4*
92 (3%) (Fig. 1C and Fig. S1B), which also identify effector cells. In the *CD4+* T cell population, a Th1
93 response was apparent, as assessed by the expression of the Th1 lineage marker, *TBX21* (13% of CD4 T
94 cells), and the Th1 cytokines, *TNF* (18%) and *IFNG* (6%). *FOXP3+ CD4+* regulatory T cells represented
95 a relatively abundant CD4 T cell population (22%), and characteristically co-expressed *IL2RA*, *PD-1* and
96 *CTLA4*. *CD4+* T follicular helper T cells (Tfh cells) were identified by their expression of *BCL6* (2%),
97 *IL-21* (1%), and the chemokine receptor, *CXCR5* (2%) (Fig. 1C and Fig. S1C-D). In summary, the PDAC
98 tumors contained activated CD8 and CD4 T cells, including Tfh cells of presumed germinal center origin.

99 The B cell cluster (n=963 cells) was defined by the expression of the pan B cell markers, *CD19* and
100 *CD20*. 35% of B cells expressed the naïve H chain isotype, *IgD*, and B cells that expressed isotype
101 switched *IgG1* (19%) were also present (Fig. 1C). Additional evidence for an active intratumoral B cell
102 response was indicated by the presence of germinal center B cells, as assessed by their expression of
103 *BCL6* (4%) and *AICDA* (1%), the latter of which mediates SHM and isotype switching (Fig. 1C and Fig.
104 S1E). PCs (n=1984) were identified by the makers, *J chain*, *PRDM1*, and *CD138*, and high expression of
105 Ig H and L chains (Fig. 1C). Most PCs (95% of PCs) no longer expressed *CD19*, indicating they were
106 relatively mature PCs rather than plasmablasts. Thus, PDAC tumors contained activated B cells and
107 terminally differentiated PCs.

108 We further obtained histopathology images from the four resected PADC samples which we have
109 performed scRNA-Seq. We have observed presence of multiple TLS-like structures in each tumor
110 sample, with TLSs typically located in the tumor border (Fig. 1D and Fig.S2). This observation supports
111 that the B and T cell response revealed by scRNA-Seq may take place inside those TLSs.

112 **Igs from PCs in PDAC featuring isotype switching, somatic hypermutation and clonal expansion**

113 A total of 615 PCs with paired H and L chains were detected in six PDAC samples (Fig. 2A and Fig.
114 S3A). A minority of PCs (0-17%) expressed the *IgM* isotype, while the majority had undergone class
115 switching to *IgG1*, *IgG2*, *IgA2*, or *IgA1* isotypes (Fig. 2B and Fig. S3B). Analyzing SHM in the V regions
116 revealed an average of 23 and 15 mutations in the H and L chains, respectively (Fig. 2C). These rates of
117 SHM are comparable to those in antibodies induced by viral infections (*9*). Expanded PC clones were
118 identified in four of the six PDAC samples, with clone sizes ranging from 2 to 46. Strikingly, in patients
119 19 and 20, more than half of the Ig-paired PCs were products of clonal expansion (Fig. 2D). Analysis of
120 the evolution of V region SHM sequences revealed that most PCs originated from single expanded
121 nodules, although additional lineage evolutions were present (Fig. 2E and Fig. S3C), consistent with
122 typical germinal center reactions. Fewer B cells with paired Igs were sequenced (n=473), likely due to
123 lower Ig expression, which yielded only four small, expanded clones (clone size 2-3). Therefore, PCs in
124 PDAC likely arose from germinal center reactions in the PDAC stroma.

125 **Antibodies from PCs binding to intracellular self-antigens**

126 Forty-one antibodies with paired H and L chains from the six PDAC patients were selected for
127 recombinant antibody synthesis. These antibodies included the mostly expanded PC cell clones, as well as
128 some single-clone PC and B cells, and represented the products of 235 PCs and 12 B cells (Fig. 3A and
129 Table S2). Immunofluorescent staining of human PDAC cell lines and tumors was used to screen the
130 reactivity of the recombinant antibodies. Twenty-five of the 41 antibodies showed positive binding to
131 PDAC cell lines, with the expanded clones showing more frequent binding (Fig. 3A). Recombinant
132 antibodies reacted with antigens in all sub-cellular locations, including cytoplasmic (e.g. 8-3 and 15-7),
133 cytoplasmic-enriched (e.g. 19-1), both cytoplasmic and nuclear (e.g. 19-4), and nuclear-enriched

134 reactivities (e.g. 19-3 and 20-1) (Fig. 3B-C and Fig. S4). We did not identify any antibodies staining cell
135 surface antigens. Antibodies derived from a single patient's PDAC tumor could exhibit diverse staining
136 patterns (for example, 19-1 and 19-3), indicating the occurrence of an adaptive immune response to
137 multiple intracellular antigens in the same patient. All the reactive antibodies could stain multiple PDAC
138 cell lines with a similar staining pattern, as well as non-tumor human pancreatic ductal cell line, HPDE,
139 and human fibroblasts (Fig. 3D and Fig. S5). When staining PDAC tumors from which antibody
140 sequences were derived, the antibodies bound both to cancer cells and stromal cells (Fig. 3E). Thus, non-
141 mutated, non-cancer cell-specific intracellular antigens drive common humoral immune responses in
142 human PDAC.

143 **Identification of antigens driving PC cell response in PDAC**

144 Three PDAC antigens were identified by using antibody-mediated immunoprecipitation from MiaPaca2
145 cell lysates, followed by mass spectrometry analysis. Antibody 8-3, which was derived from the most
146 expanded PC clone (clone size 20) from patient 8, recognized a cortical structure in MiaPaca2 cells (Fig.
147 3C). This antibody immunoprecipitated a major protein band of approximately 45 kDa, which was
148 identified as ACTIN by mass spectrometry, as well as the ACTIN associated proteins, MYH10 and
149 MYH9 (Fig. 4A). Antibody 8-3 co-localized with filamentous actin (F-actin) in the cell cortex, and its
150 antigen re-localized to perinuclei foci after treatment with the actin destabilizing drug, cytochalasin D
151 (Fig. 4B). Knockdown of ACTIN with siRNA reduced staining by antibody 8-3, but not staining by a
152 MYH10-specific antibody (Fig. S6A), indicating that ACTIN was the target of antibody 8-3. This
153 antibody was confirmed to bind to polymerized F-actin, but not monomeric G-actin, using in vitro actin
154 polymerization and depolymerization assays (Fig. 4C). We developed an F-actin specific ELISA and
155 measured the EC_{50} of antibody 8-3 for F-actin to be 9.1 nM, a relatively high affinity/avidity that was
156 probably a result of SHM (Fig. 4D and Fig. 2E). Sequencing the actin genes (ACTB and ACTG1) from
157 the tumor organoid derived from patient 8, the source of the PCs encoding antibody 8-3, showed no
158 mutations in the protein-coding regions, confirning the self-antigen nature.

159 Similarly, antibody 19-3, the second most expanded PC clone in patient 19 (clone size 23),
160 immunoprecipitated a protein complex of RUVBL1 and RUVBL2, as determined by mass spectrometry.
161 Knockdown of RUVBL2 reduced antibody 19-3 binding in the MiaPaca2 cell line (Fig. 4F and Fig. S6B).
162 This antibody recognized recombinant RUVBL2 but not RUVBL1 protein, with an EC_{50} of 0.2 uM (Fig.
163 4G and Fig. S6C), confirming that antibody 19-3 recognizes RUVBL2.
164 Antibody 15-7, which was derived from a single PC clone in the tumor from patient 15, co-stained with
165 antibodies specific for the mitochondrial markers, COX4I1 and HSPA9 (Fig. S6D). This antibody
166 recognized a mitochondrial-enriched protein band with an apparent molecular weight of 60 kDa (Fig.
167 4H), which was identified as heat-shock protein D1 (HSPD1) by mass spectrometry. HSPD1 was
168 confirmed to be the antigen of antibody 15-7 by immunofluorescent co-localization in MiaPaca2 cells,
169 siRNA knockdown, and recombinant protein binding, with an EC_{50} of 7.9 nM (Fig. 4I-J and Fig. S6D).
170 In summary, our identification of three self-antigens, including antigens for two antibodies from highly
171 expanded PC clones, indicates that widely expressed, intracellular self-antigens may be targets of humoral
172 immune responses in human PDAC.

173 **The frequent occurrence of antibody responses to F-actin and HSPD1 in PDAC patients**

174 We collected plasma samples from 59 PDAC patients and 61 healthy donors, and measured IgG titers to
175 F-actin, RUVBL2, and HSPD1, respectively (Table S3). Demographics, such as gender, age, and race, did
176 not significantly affect antibody concentration. Interestingly, plasma from normal donors contained
177 detectable levels of IgG responses to these three antigens. In PDAC, the IgG F-actin and HSPD1 antibody
178 titers were significantly higher than those in normal individuals (Fig. 4K and Fig. S7A). IgG F-actin
179 antibody titers were significantly reduced in patients who had received neoadjuvant therapy, but this was
180 not observed for either HSPD1 or RUVBL2 antibody titers (Fig. S7B), suggesting that B cell responses
181 for different antigens may have different sensitivities to cytotoxic chemotherapy. These antibody
182 responses did not correlate with other pathological features such as tumor stage, size or grade. Thus,
183 PDAC patients likely promote auto-antibody responses which pre-exist in healthy donors.

184 **DISCUSSION**

185 PDAC is generally considered to be one of the more immunologically "silent" carcinomas and to be
186 resistant to cancer immunotherapy for this reason. Reports, however, of TLSs in PDAC (*2-4*), of
187 neoantigens with homology to infectious disease-derived peptides in long-term survivors of PDAC (*6*),
188 and of signs of improved anti-PDAC immunity in metastatic lesions of patients with PDAC after
189 inhibition of CXCR4 (*5*), all point to a need for a deeper understanding of the relationship between this
190 cancer and the immune system. The antigens driving the B cell response are more readily identified by the
191 Ig product of the B cells and PCs. Thus, we chose to interrogate the Ig products of intratumoral B/PCs in
192 PDAC.

193 Our scRNA-Seq analysis of CD45+ immune cells in primary PDAC samples indicated active
194 intratumoral immune reactions, such as the presence of effector CD8 T cells expressing *PRF1*, *GZMB*,
195 and *IFNG*, and effector CD4 T cells expressing *TNF* and *IFNG*. We were able to confirm the four
196 resected PDAC tumor samples as being microsatellite-stable, representing the majority of PDAC (*10*).
197 The presence of effector T cells in our cohort is consistent with previous studies of human and mouse
198 autochthonous PDAC immune microenvironments in which activated, effector T cells were found (*11*). In
199 addition, scRNA-Seq identified CD4 T cells with the Tfh phenotype by their transcriptional expression of
200 *BCL6* and *CXCR5*, and germinal center B cells expressing *BCL6*. The presence of a B cell response is
201 further supported by Ig sequencing that identified isotypically switched, somatically hypermutated and
202 expanded PC clones. The presence of TLS in PDAC stroma from the paired histology images further
203 support the integrated B and T cell responses. It is interesting that these indicators of an active adaptive
204 immune reaction are occurring despite the presence of large proportion of FOXP3-expressing regulatory
205 T cells.

206 There are a few previous studies exploring the antigen reactivity of B cells and PCs in other tumors
207 (*12, 13*), but our study is the first to apply this approach to PDAC. While we were unsuccessful in our
208 initial intent to discover tumor-specific B cell antigens, the finding of Igs from PCs frequently binding to
209 widely expressed, non-mutated intracellular self-antigens in human PDAC is intriguing. Our screening in

210 PDAC identified most antibodies as recognizing intracellular antigens that were shared by multiple
211 PDAC cell lines, normal epithelial cells and fibroblasts. This conclusion was confirmed by the
212 identification of three self-antigens, F-actin, RUVBL2 and HSPD1, as targets of these humoral immune
213 responses. All the seven PDAC patients enrolled for this study have no records of auto-immune disease or
214 pancreatitis. In this context, it is worth noting that 20% of naïve B cells in human peripheral blood are
215 reported to be autoreactive (*14*), which is consistent with our detection of autoantibody responses to those
216 antigens in healthy donors. Self-reactive B cell responses are likely promoted in PDAC because of
217 continual exposure of intracellular self-antigens through cell death and chronic inflammation, reminiscent
218 of the antibody responses in autoimmune diseases. Autoantibody responses to F-actin, RUVBL2 and
219 HSPD1 have been reported in various autoimmune conditions (*15-17*) and cancers (*18, 19*). Previously,
220 immunization with mouse syngeneic ES cells reduce mouse pancreatic tumor progression, indicating self-
221 antigens likely drive such immune response (*7, 8*). Additionally, a recent study reported that the self-
222 protein matrix metallopeptidase 14 was a major auto-antigen in human ovarian cancer, and some Igs were
223 likely originated from germline encoded auto-reactive B cell (*13*). Thus, the B cell response to self-
224 antigens may be a common feature of cancer.
225 Our analysis of plasma titer to F-actin, RUVBL2 and HSPD1 did reveal that PDAC patients have
226 significantly higher titers to F-actin and HSPD1 as compared to a group of healthy donors. Our analysis
227 did not reveal a significant correlation with tumor-associated pathological factors, although this may be
228 partially due to our relatively small cohort of patients. Our studies can be potentially strengthened by
229 analyzing serial tumor biopsies and plasma obtained during the course of tumor progression or response
230 to therapy such as CXCR4 inhibition, thus providing more dynamic pictures of B cell response and
231 antibody titer changes.
232 One open question from this study is whether the B cell response to intracellular self-antigens affects
233 PDAC progression. Given the generally positive correlation of a B cell response with a favorable outcome
234 in PDAC (*2-4*), we speculate that those autoreactive B cell responses may indirectly have an anti-tumor
235 role. While antibodies binding intracellular antigens cannot directly target live tumor cells, these antigens

236 can be exposed to antibody binding during cancer cell death, such as necrosis, and potentially induce
237 inflammation through complement activation and Fc receptor binding. Moreover, we expect that B cells
238 binding such self-antigens will internalize and engage in antigen presentation to CD4+ T cells. F-actin has
239 been reported to promote antigen presentation through the F-actin receptor Clec9A on dendritic cells in
240 breast cancer model (*20*). Further understanding the B cell response in PDAC may potentially provide
241 opportunities for modulation of cancer immunotherapy. In any event, the finding of T cell and B cell
242 responses in the PDAC tumors indicates that an adaptive immune response is occurring in the tumor
243 microenvironment, which may be exploited for tumor control.

244 **MATERIALS AND METHODS**

245 **Study design**

246 This study is designed to study B cell response and identify B cell targeted antigens in human PDACs.
247 This study consists of :1) ScRNA-Req of immune cells infiltrating human PDAC and Igs of B and
248 plasma cells; 2) Synthesizing of recombinant antibodies from Ig sequencing; 3) Screening of recombinant
249 antibodies reactivities toward PDAC cell lines and tumor tissues; 4) Identification of antigens. This
250 pipeline was used to study four resected and three FNA naïve-treated PDAC samples. The antibodies
251 synthesizing and screening aim to profile the most expanded plasma cells clones in PDAC to get a better
252 picture of B cell reactivity in human PDAC.

253 **Human samples**

254 All human samples were obtained with written consent and IRB approval. Four resected PDAC
255 specimens and three FNA (two passes each) specimens were obtained from Northwell Health. Archived
256 plasma samples from PDAC patients (n=59) were received from Northwell Health. Plasma samples from
257 healthy donors (n=61) were obtained from volunteer donors or purchased from commercial resources
258 (Innovative Research and BioChemed Services). Microsatellite instability status of resected PDAC
259 samples were determined by immunohistochemistry staining of MLH1, MSH2, MSH6 and PMS2,
260 performed and interpreted by pathologists from Northwell Health. Histopathologic hematoxylin and eosin

261 images were obtained from Northwell pathology department acquired by Leica Aperio slide scanner. All
262 patient samples were de-identified.

263 **Cell lines and culture**

264 Human PDAC cell lines MiaPaca2, Suit2, Panc-1, and foreskin fibroblast (BJ-hTert) were obtained from
265 Cold Spring Harbor Laboratory cell validation center, and had been validated by short tandem repeat
266 profiling. The normal human pancreatic ductal epithelial cell line (HPDE) was obtained from Dr. Krainer
267 lab in CSHL, originally purchased from Kerafast. All cell lines had been tested mycoplasma free and
268 cultured in the conditions recommended by ATCC or the manufacturer.

269 **Tumor samples preparation and Single-cell sequencing**

270 A small portion of the resection tumor was snap-frozen for histology. The remaining human PDAC tumor
271 samples were digested into single cells using collagenases and about 10% of single cells digest was used
272 for tumor organoid culture as described (*21*). Live immune cells were sorted by $EpCAM^{-}$ /$CD45^{+}$
273 (Biolegend, # clone 2D1 and 9C4) on a Sony SH800 cell sorter. About 10,000 immune cells were
274 barcoded with 10X Genomics Chromium single cell 5' kit, and both gene expression and Ig libraries were
275 prepared and sequenced according to the 10X Genomics manual.

276 **Sequencing data analysis**

277 The scRNA-Seq and Ig reads were aligned and quantified using the Cell Ranger pipeline (10X Genomics,
278 version 6.0.0). Dead cells and cells with the number of genes expressed less than 200 were also filtered
279 out. ScRNA-Seq Data was normalized, logarithm transformed and scaled. Doublets were removed using a
280 R package 'Scrublet'. Principle component analysis (PCA) was run with 50 components using the top
281 4000 genes of each sample. The nearest neighbor algorithm was run with 50 PCAs and clustered in
282 UMAP projections using Leiden clustering. All additional analyses were performed using Loupe Browser
283 (10X Genomics, version 6.1.0) and the Python toolkit Scanpy 1.6.0. Immune cells clusters were defined
284 using the set of markers and UMAP clusters: T cells ($CD3^{+}$, TCR^{+}, $NCAM^{-}$), NK cells ($CD3^{-}$, $NCAM^{+}$),
285 B cells ($CD20^{+}$, $CD79A^{+}$, $IgKC^{low}$), PCs ($JChain^{hi}$, $IgKC^{hi}$), myeloid cells ($CD14^{+}$, $CSF1R^{+}$), mast cells

286 (CPA3$^+$, GATA2$^+$), fibroblasts (FAP$^+$, ACTA2$^+$, PDGFRA1$^+$), epithelial cells (CK19$^+$, CK18$^+$, CK5$^+$,
287 CK14$^+$).

288 **Ig data analysis**

289 PCs and B cells clusters defined by scRNA-Seq were used to select cell type specific Igs analysis. In one
290 patient (Pt-15), gene expression sequencing data was not available, the PCs were defined by high
291 expression of H chain (UMI>=100). B or PC specific Igs were exported from the Loupe V(D)J Browser
292 (10X Genomics, version 4.0.0) and analyzed for isotypes and clonotypes. For somatic hypermutation
293 analysis, V region sequences were analyzed by Igblast (NCBI) and visualized by Graphpad Prism 5
294 (Dotmatics). For lineage tree analysis, Ig sequences were first analyzed using R packages Change-O and
295 alakazam (*22*), and the Ig lineages were built using a R package PHYLIP. Finally, Lineage trees were
296 visualized using a R package igraph.

297 **Recombinant Antibodies production**

298 The selected antibody V(D)J sequences were synthesized from IDT, and cloned into pFUSEss H and L
299 vectors (Invivogen) using NEB HIFI assembly kit (NEB, #5520s). The heavy chains were cloned into
300 human IgG1 or customer-designed human IgG4-His vector. A 6x His tag with a Gly-Ser-Gly linker was
301 inserted before the stop codon of human IgG4 constant region, synthesized and replaced the IgG1 in
302 pFUSE-CHIg-hG1 vector. The light chain was cloned into a vector containing IgKC, IgLC2, or
303 costumed-made IgLC1 vector, to match the original light chain. Sequences confirmed antibody vectors
304 were mixed at H:L 1:1.5 ratio, and transiently transfected into 293T cells, cultured in 10% IgG reduced
305 serum. Culture supernatants were collected four days later and antibodies were purified using the Protein
306 G column (Thermo Fisher, #89956). The antibodies were further concentrated and the buffer was
307 exchanged into PBS using Amicon 50K centrifugal filter device (Sigma, #UFC805096). The antibody
308 concentration was quantified by NanoDrop (Thermo Fisher) and human IgG ELISA kit (Mabtech, #3850-
309 1H-6).

310 **Antibody screening using immunofluorescent staining**

311 Cells were seeded in the 24-well glass-bottom cell culture plate (Chemglass, #CLS-1812-024), and used
312 2-3 days later at 50-80% confluency. Cells were fixed with 4% PFA, permeabilized with 0.1% Triton-
313 X100, blocked with 3% FBS, and stained with 10 ug/ml human query antibodies diluted in PBST
314 containing 1% FBS overnight at 4 °C. Cells were then washed three times with PBST, and stained with
315 fluorescent conjugated secondary anti-human IgG antibody (Thermo Fisher, #A21090 and #A-11013) and
316 DNA dye DAPI. In human tumor section staining, anti-His secondary antibody (Biolegend, #362607) was
317 used to detect IgG4-His primary antibodies. Other antibodies and dyes used were: Phalloidin (Thermo
318 Fisher, #A12379), MYH10 (Atlas Antibodies, #HPA047541), cytochalasin D (Thermo Fisher,
319 #PHZ1063), ACTIN (Cell Signaling Technology, #3700S), RUVBL2 (Atlas Antibodies, #HPA067966),
320 RUVBL1 (Atlas Antibodies, # HPA019947), HSPD1 (Atlas Antibody, #HPA050025), HSPA9 (Atlas
321 Antibody, #HPA000898), COX4I1 (Atlas antibody, #HPA002485), KRT19 (Abcam, #ab203445), human
322 IgG isotype controls (Biolegend, #403502 and #403702). The samples were imaged in Leica SP8
323 confocal microscope under 40x magnification. Antibody screening images were acquired using the same
324 confocal setting for isotype control staining, and the gain of query antibodies was reduced if images were
325 saturated in the setting. Images were analyzed using Leica LAS X or Image J software.

326 **Immunoprecipitation and mass spectrometry**

327 Antibodies were covalently crosslinked to magnetic beads using the Thermo Fisher Dynabeads Antibody
328 Coupling Kit. The total cell lysate was prepared from MiaPaca2 cell line using TNET lysis buffer (50 mM
329 Tris-HCl, pH 7.5, 150 mM NaCl, 5 mM EDTA and 1% Triton X-100). Dynabeads containing 2-5 ug
330 crosslinked antibodies or isotype control were first blocked with 1%BSA, then incubated with up to 1mg
331 cell lysate overnight in 4C in TNET buffer. The beads were separated using a magnetic rack, washed
332 three times with TNET buffer (or with increased NaCl concentration), and eluted with 2X SDS under
333 boiling. The immunoprecipitation elute was running in gradient SDS-PAGE gel and stained with a silver
334 staining kit (Thermo Fisher, #24600).

335 Distinct gel bands were excised, de-stained, reduced with 3 mM TCEP and alkylated with 10 mM
336 CEMTS, and then digested with trypsin. Eluting peptides were ionized and transferred into an Exploris

337 Orbitrap mass spectrometer (Thermo Fisher). Spectral data were searched against the human database and
338 a database of common contaminants. M-oxidation and N/Q-deamidation were set as variable
339 modifications. Peptide-spectral matches were filtered to maintain FDR <1% using the Percolator.

340 **siRNA knockdown**

341 Cells were transfected with control or siRNA at 20-60uM, cultured for three days, and proceeded for
342 immunofluorescent staining. siRNA against human ACTB (#SASI_Hs01_00204238,
343 #SASI_Hs01_00204239), MYH10 (#SASI_Hs01_00072460, #SASI_Hs02_00340636), MYH9
344 (#SASI_Hs01_00197338, #SASI_Hs01_00197339), RUVBL2 (GATGATTGAGTCCCTGACCAA,
345 GAAGATGTGGAGATGAGTGAG), control (GGATGTAAGTGGGAAAGTGGA) were purchased
346 from Sigma. siRNA targeting HSPD1 (L-010600-00-0005) was purchased from Horizon Discovery.

347 **Actin polymerization or de-polymerization and dot-blot assay**

348 Human non-muscle actin (Cytoskeleton, # APHL99) was polymerized or de-polymerized according to the
349 manufacturer's protocol. Briefly, actin was first diluted into 0.4 mg/ml in G-buffer (5 mM Tris-HCl, 0.2
350 mM $CaCl_2$, 0.2 mM ATP), and kept in ice for 1h. For polymerization, 10% polymerization buffer (500
351 mM KCl, 20 mM MgCl2) with 1 mM final ATP and 5uM phalloidin (Simga, #P2141) was added to the
352 actin and incubated at room temperature for 1h. For de-polymerization, 5 uM latrunculin B (Sigma,
353 #428020) was added into the actin with G-buffer, and incubated in ice for 1h. Actin samples were further
354 diluted into G-buffer or polymerization buffer supplemented with phalloidin or Latrunculin B, and serial
355 dilutions of F-actin or G-actin were blotted on nitrocellulose membrane using Bio-Dot microfiltration
356 apparatus (Bio-Rad) according to the manufacturer's instructions. The membrane was furthered blocked
357 and incubated with human IgG4 isotype control, Ab 8-3, mouse anti-human Actin antibody (Thermo
358 Fisher, # MA1-140) at 1 ug/ml for 1h, washed and detected with HRP conjugated anti-human IgG
359 (Thermo Fisher, #A18811) or anti-mouse IgG (Biolegend, #405306) secondary antibody, and developed
360 by ECL substrate.

361 **ELISA**

362 Recombinant proteins RUVBL2 (Creative Biomart, #RUVBL2-30950), RUVBL1 (Novus, #NBP1-
363 50845), HSPD1 (Origene, #TP760396), or BSA control were coated in PBS with 0.25 ug per well in 96-
364 well ELISA plate (Corning) overnight in 4C. The plate was blocked with 1% BSA, washed with PBST,
365 incubated with query antibodies or isotype control at 1 ug/ml diluted in 0.1% BSA in PBST for 1h,
366 detected with HRP conjugated secondary antibody (1ug/ml), and developed by TMB substrate
367 (Biolegend, #421101) for 5-10 min. For F-actin ELISA, polymerized F-actin was diluted in
368 polymerization buffer supplemented with 5uM phalloidin and 1mM ATP, and coated in the ELISA plate
369 for 1h at room temperature, followed by antibody binding and development.
370 For human plasma studies, the antigens were coated as above, then blocked with 5% milk in PBS.
371 PDAC or healthy donor plasma was diluted 1/100 and 1/1000 in 0.5% milk in PBST, and each sample
372 was run in duplicates. Positive controls are using antibodies 8-3, 19-3 or 15-7. Background signal was
373 obtained using the higher signal from secondary antibody only and plate coated with BSA. All samples to
374 the same antigen were analyzed at the same time to avoid batch differences. Each ELISA analysis was
375 repeated twice.
376 **Mitochondria cell fraction and western blot**
377 For crude mitochondria fraction, the cells were first lysed using low salt buffer (0.25 M sucrose, 20 mM
378 HEPES-KOH pH 7.5, 10 mM KCl, 1.5 mM MgCl2, 1 mM EDTA, 1 mM EGTA, 1 mM DTT)
379 supplemented with proteinase/phosphatase inhibitors, homologized with a Teflon-glass homogenizer, and
380 then centrifuged at 700 g for 10 min in 4C to collect the cytosol fraction in the supernatant. The cytosol
381 fraction was further centrifuged at 10,000 g for 15 min to collect the mitochondria fraction in the pellet.
382 Same amounts of SDS-reduced cytosol or mitochondria fractions were run in western blot, and detected
383 with antibody 15-7, HSPA9 and GAPDH (Cell Signaling Technology, #97166). A separate sample gel
384 was silver stained and cut around 60kd for mass spectrometry analysis.
385 **Histopathology image analysis**

386 The scanned resected PDAC histopathologic images were opened with ImageScope (Leica), and
387 lymphocytes aggregates with bigger than 0.01 mm^2 size were counted and exported for size
388 measurement using image J.

389 **Statistical analysis**

390 Statistical analysis was performed using Graphpad Prism 5. The plasma IgG data was first tested for
391 normality distribution in Graphpad. Mann-Whitney t-test was used for a two-group comparison of non-
392 normal distribution data, Kruskal-Wallis ANOVA test was used for comparisons of three or more groups
393 of non-normal distribution data. Fisher's test was used for demographic factors comparison, and
394 Pearson's correlation was used for correlation studies. $P<0.05$ was used for statistical significance.

395 **List of Supplementary Materials**

396 Fig. S1 Characterization of primary PDAC immune cells microenvironment by scRNA-Seq
397 Fig. S2. Presence of TLS like structures in PDAC.
398 Fig. S3 Additional Ig sequences evolution trees from PCs in PDAC
399 Fig. S4 Antibodies staining atlas on MiaPaca2 cell line.
400 Fig. S5 Examples of antibodies staining in PDAC and non-cancer cell lines
401 Fig. S6 Characterization of antibodies 8-3, 19-3 and 15-7
402 Fig. S7 Comparison of plasma IgG titers to F-actin, RUVBL2 and HSPD1 between healthy donors and
403 PDAC patients.
404 Table S1 Human PDAC samples information for scRNA-Seq studies.
405 Table S2 List of antibodies synthesized and screening results.
406 Table S3 Human samples information for plasma studies.

407 **References and Notes**

408 1. A. S. Bear, R. H. Vonderheide, M. H. O'Hara, Challenges and Opportunities for Pancreatic Cancer
409 Immunotherapy. *Cancer Cell* **38**, 788-802 (2020).
410 2. N. Hiraoka, Y. Ino, R. Yamazaki-Itoh, Y. Kanai, T. Kosuge, K. Shimada, Intratumoral tertiary
411 lymphoid organ is a favourable prognosticator in patients with pancreatic cancer. *Br J Cancer*
412 **112**, 1782-1790 (2015).

413 3. G. F. Castino, N. Cortese, G. Capretti, S. Serio, G. Di Caro, R. Mineri, E. Magrini, F. Grizzi, P.
414 Cappello, F. Novelli, P. Spaggiari, M. Roncalli, C. Ridolfi, F. Gavazzi, A. Zerbi, P. Allavena, F.
415 Marchesi, Spatial distribution of B cells predicts prognosis in human pancreatic adenocarcinoma.
416 *Oncoimmunology* **5**, e1085147 (2016).
417 4. J. G. A, V. Rajamanickam, C. Bui, B. Bernard, J. Pucilowska, C. Ballesteros-Merino, M. Schmidt, K.
418 McCarty, M. Philips, B. Piening, C. Dubay, T. Medler, P. Newell, P. Hansen, E. Tran, E. Tang, C.
419 Bifulco, M. Crittenden, M. Gough, K. H. Young, Germinal center reactions in tertiary lymphoid
420 structures associate with neoantigen burden, humoral immunity and long-term survivorship in
421 pancreatic cancer. *Oncoimmunology* **10**, 1900635 (2021).
422 5. D. Biasci, M. Smoragiewicz, C. M. Connell, Z. Wang, Y. Gao, J. E. D. Thaventhiran, B. Basu, L.
423 Magiera, T. I. Johnson, L. Bax, A. Gopinathan, C. Isherwood, F. A. Gallagher, M. Pawula, I.
424 Hudecova, D. Gale, N. Rosenfeld, P. Barmpounakis, E. C. Popa, R. Brais, E. Godfrey, F. Mir, F. M.
425 Richards, D. T. Fearon, T. Janowitz, D. I. Jodrell, CXCR4 inhibition in human pancreatic and
426 colorectal cancers induces an integrated immune response. *Proc Natl Acad Sci U S A* **117**, 28960-
427 28970 (2020).
428 6. V. P. Balachandran, M. Luksza, J. N. Zhao, V. Makarov, J. A. Moral, R. Remark, B. Herbst, G.
429 Askan, U. Bhanot, Y. Senbabaoglu, D. K. Wells, C. I. O. Cary, O. Grbovic-Huezo, M. Attiyeh, B.
430 Medina, J. Zhang, J. Loo, J. Saglimbeni, M. Abu-Akeel, R. Zappasodi, N. Riaz, M. Smoragiewicz, Z.
431 L. Kelley, O. Basturk, I. Australian Pancreatic Cancer Genome, R. Garvan Institute of Medical, H.
432 Prince of Wales, H. Royal North Shore, G. University of, H. St Vincent's, Q. B. M. R. Institute, C. f.
433 C. R. University of Melbourne, I. f. M. B. University of Queensland, H. Bankstown, H. Liverpool, C.
434 O. B. L. Royal Prince Alfred Hospital, H. Westmead, H. Fremantle, H. St John of God, H. Royal
435 Adelaide, C. Flinders Medical, P. Envoi, H. Princess Alexandria, H. Austin, I. Johns Hopkins
436 Medical, A. R.-N. C. f. A. R. o. Cancer, M. Gonen, A. J. Levine, P. J. Allen, D. T. Fearon, M. Merad,
437 S. Gnjatic, C. A. Iacobuzio-Donahue, J. D. Wolchok, R. P. DeMatteo, T. A. Chan, B. D. Greenbaum,
438 T. Merghoub, S. D. Leach, Identification of unique neoantigen qualities in long-term survivors of
439 pancreatic cancer. *Nature* **551**, 512-516 (2017).
440 7. N. G. Kooreman, Y. Kim, P. E. de Almeida, V. Termglinchan, S. Diecke, N. Y. Shao, T. T. Wei, H. Yi,
441 D. Dey, R. Nelakanti, T. P. Brouwer, D. T. Paik, I. Sagiv-Barfi, A. Han, P. H. A. Quax, J. F. Hamming,
442 R. Levy, M. M. Davis, J. C. Wu, Autologous iPSC-Based Vaccines Elicit Anti-tumor Responses In
443 Vivo. *Cell Stem Cell* **22**, 501-513 e507 (2018).
444 8. X. Ouyang, Y. Liu, Y. Zhou, J. Guo, T. T. Wei, C. Liu, B. Lee, B. Chen, A. Zhang, K. M. Casey, L.
445 Wang, N. G. Kooreman, A. Habtezion, E. G. Engleman, J. C. Wu, Antitumor effects of iPSC-based
446 cancer vaccine in pancreatic cancer. *Stem Cell Reports* **16**, 1468-1477 (2021).
447 9. R. Di Niro, L. Mesin, N. Y. Zheng, J. Stamnaes, M. Morrissey, J. H. Lee, M. Huang, R. Iversen, M. F.
448 du Pre, S. W. Qiao, K. E. Lundin, P. C. Wilson, L. M. Sollid, High abundance of plasma cells
449 secreting transglutaminase 2-specific IgA autoantibodies with limited somatic hypermutation in
450 celiac disease intestinal lesions. *Nat Med* **18**, 441-445 (2012).
451 10. C. Luchini, L. A. A. Brosens, L. D. Wood, D. Chatterjee, J. I. Shin, C. Sciammarella, G. Fiadone, G.
452 Malleo, R. Salvia, V. Kryklyva, M. L. Piredda, L. Cheng, R. T. Lawlor, V. Adsay, A. Scarpa,
453 Comprehensive characterisation of pancreatic ductal adenocarcinoma with microsatellite
454 instability: histology, molecular pathology and clinical implications. *Gut* **70**, 148-156 (2021).
455 11. E. Elyada, M. Bolisetty, P. Laise, W. F. Flynn, E. T. Courtois, R. A. Burkhart, J. A. Teinor, P. Belleau,
456 G. Biffi, M. S. Lucito, S. Sivajothi, T. D. Armstrong, D. D. Engle, K. H. Yu, Y. Hao, C. L. Wolfgang, Y.
457 Park, J. Preall, E. M. Jaffee, A. Califano, P. Robson, D. A. Tuveson, Cross-Species Single-Cell
458 Analysis of Pancreatic Ductal Adenocarcinoma Reveals Antigen-Presenting Cancer-Associated
459 Fibroblasts. *Cancer Discov* **9**, 1102-1123 (2019).

460 12. J. DeFalco, M. Harbell, A. Manning-Bog, G. Baia, A. Scholz, B. Millare, M. Sumi, D. Zhang, F. Chu,
461 C. Dowd, P. Zuno-Mitchell, D. Kim, Y. Leung, S. Jiang, X. Tang, K. S. Williamson, X. Chen, S. M.
462 Carroll, G. Espiritu Santo, N. Haaser, N. Nguyen, E. Giladi, D. Minor, Y. C. Tan, J. B. Sokolove, L.
463 Steinman, T. A. Serafini, G. Cavet, N. M. Greenberg, J. Glanville, W. Volkmuth, D. E. Emerling, W.
464 H. Robinson, Non-progressing cancer patients have persistent B cell responses expressing
465 shared antibody paratopes that target public tumor antigens. *Clin Immunol* **187**, 37-45 (2018).
466 13. R. D. Mazor, N. Nathan, A. Gilboa, L. Stoler-Barak, L. Moss, I. Solomonov, A. Hanuna, Y. Divinsky,
467 M. D. Shmueli, H. Hezroni, I. Zaretsky, M. Mor, O. Golani, G. Sabah, A. Jakobson-Setton, N.
468 Yanichkin, M. Feinmesser, D. Tsoref, L. Salman, E. Yeoshoua, E. Peretz, I. Erlich, N. M. Cohen, J.
469 M. Gershoni, N. Freund, Y. Merbl, G. Yaari, R. Eitan, I. Sagi, Z. Shulman, Tumor-reactive
470 antibodies evolve from non-binding and autoreactive precursors. *Cell* **185**, 1208-1222 e1221
471 (2022).
472 14. H. Wardemann, S. Yurasov, A. Schaefer, J. W. Young, E. Meffre, M. C. Nussenzweig, Predominant
473 autoantibody production by early human B cell precursors. *Science* **301**, 1374-1377 (2003).
474 15. A. Granito, L. Muratori, P. Muratori, G. Pappas, M. Guidi, F. Cassani, U. Volta, A. Ferri, M. Lenzi,
475 F. B. Bianchi, Antibodies to filamentous actin (F-actin) in type 1 autoimmune hepatitis. *J Clin*
476 *Pathol* **59**, 280-284 (2006).
477 16. K. Kaji, N. Fertig, T. A. Medsger, Jr., T. Satoh, K. Hoshino, Y. Hamaguchi, M. Hasegawa, M. Lucas,
478 A. Schnure, F. Ogawa, S. Sato, K. Takehara, M. Fujimoto, M. Kuwana, Autoantibodies to RuvBL1
479 and RuvBL2: a novel systemic sclerosis-related antibody associated with diffuse cutaneous and
480 skeletal muscle involvement. *Arthritis Care Res (Hoboken)* **66**, 575-584 (2014).
481 17. G. Schett, Q. Xu, A. Amberger, R. Van der Zee, H. Recheis, J. Willeit, G. Wick, Autoantibodies
482 against heat shock protein 60 mediate endothelial cytotoxicity. *J Clin Invest* **96**, 2569-2577
483 (1995).
484 18. M. H. Hansen, H. Nielsen, H. J. Ditzel, The tumor-infiltrating B cell response in medullary breast
485 cancer is oligoclonal and directed against the autoantigen actin exposed on the surface of
486 apoptotic cancer cells. *Proc Natl Acad Sci U S A* **98**, 12659-12664 (2001).
487 19. Y. He, Y. Wu, Z. Mou, W. Li, L. Zou, T. Fu, A. Zhang, D. Xiang, H. Xiao, X. Wang, Proteomics-based
488 identification of HSP60 as a tumor-associated antigen in colorectal cancer. *Proteomics Clin Appl*
489 **1**, 336-342 (2007).
490 20. E. Giampazolias, O. Schulz, K. H. J. Lim, N. C. Rogers, P. Chakravarty, N. Srinivasan, O. Gordon, A.
491 Cardoso, M. D. Buck, E. Z. Poirier, J. Canton, S. Zelenay, S. Sammicheli, N. Moncaut, S. Varsani-
492 Brown, I. Rosewell, C. Reis e Sousa, Secreted gelsolin inhibits DNGR-1-dependent cross-
493 presentation and cancer immunity. *Cell* **184**, 4016-4031 e4022 (2021).
494 21. S. F. Boj, C. I. Hwang, L. A. Baker, Chio, II, D. D. Engle, V. Corbo, M. Jager, M. Ponz-Sarvise, H.
495 Tiriac, M. S. Spector, A. Gracanin, T. Oni, K. H. Yu, R. van Boxtel, M. Huch, K. D. Rivera, J. P.
496 Wilson, M. E. Feigin, D. Ohlund, A. Handly-Santana, C. M. Ardito-Abraham, M. Ludwig, E. Elyada,
497 B. Alagesan, G. Biffi, G. N. Yordanov, B. Delcuze, B. Creighton, K. Wright, Y. Park, F. H. Morsink, I.
498 Q. Molenaar, I. H. Borel Rinkes, E. Cuppen, Y. Hao, Y. Jin, I. J. Nijman, C. Iacobuzio-Donahue, S. D.
499 Leach, D. J. Pappin, M. Hammell, D. S. Klimstra, O. Basturk, R. H. Hruban, G. J. Offerhaus, R. G.
500 Vries, H. Clevers, D. A. Tuveson, Organoid models of human and mouse ductal pancreatic
501 cancer. *Cell* **160**, 324-338 (2015).
502 22. N. T. Gupta, J. A. Vander Heiden, M. Uduman, D. Gadala-Maria, G. Yaari, S. H. Kleinstein,
503 Change-O: a toolkit for analyzing large-scale B cell immunoglobulin repertoire sequencing data.
504 *Bioinformatics* **31**, 3356-3358 (2015).

Acknowledgments:

We thank Sharon Fox and Cristina Valente and other members from Northwell Health Biospecimen Repository in helping coordinate the human sample collections. We thank Ledong Wan from Dr. Krainer lab at CSHL in providing the HPDE cell line. We thank Dr. Semir Bayez of CSHL for his thoughtful input in this project. We thank members of Fearon lab for their thoughtful discussions of this project and help review of this manuscript. This project was funded by Lustgarten Foundation and Simons Foundation awarded to Dr. Douglas Fearon.

Funding:

Lustgarten Foundation for Pancreatic Research (DF)

Simons Foundation (DF)

Author contributions:

Conceptualization: MY, DF

Methodology: MY, JP, JY, DP, PC, YZ, BH, HP, AH, DK, KP, AR, DS, MW, DT

Investigation: MY, SS, PM,

Visualization: MY, JP, YZ, BH

Funding acquisition: DF

Project administration: MY

Supervision: DF

Writing – original draft: MY, DF

Writing – review & editing: YZ, PM, KP, AR

Competing interests: Authors declare that they have no competing interests.

Data and materials availability: The sequencing data from this study will be deposited into the NCBI database. Public codes/software was used for the data analysis as described in the paper. The codes for sequencing data analysis and experimental material can be accessed through communication with the corresponding authors.

Figure 1.

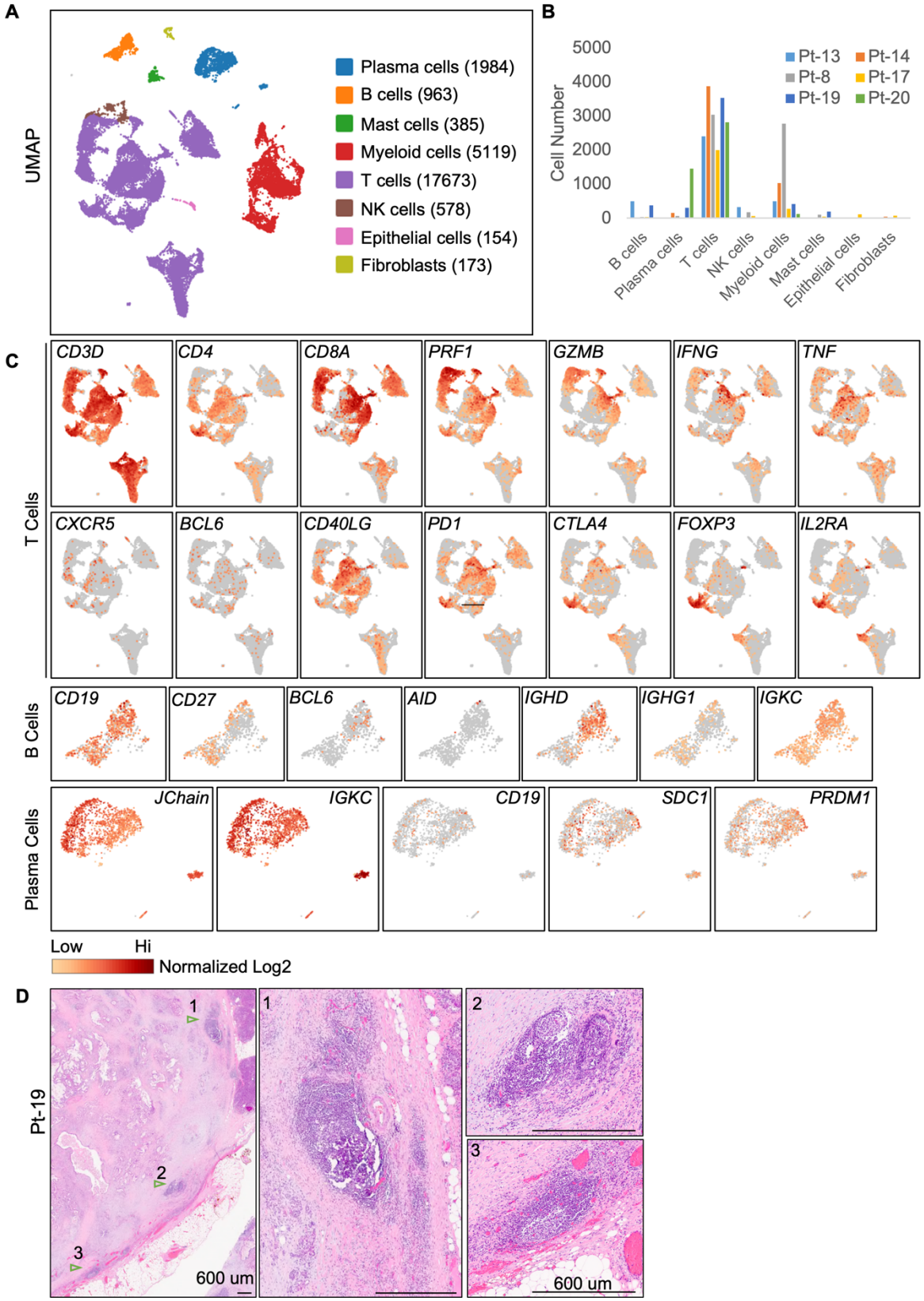
A
UMAP
Plasma cells (1984)
B cells (963)
Mast cells (385)
Myeloid cells (5119)
T cells (17673)
NK cells (578)
Epithelial cells (154)
Fibroblasts (173)
B
Cell Number
5000
4000
3000
2000
1000
0
Pt-13
Pt-14
Pt-8
Pt-17
Pt-19
Pt-20
B cells
Plasma cells
T cells
NK cells
Myeloid cells
Mast cells
Epithelial cells
Fibroblasts
C
T Cells
CD3D
CD4
CD8A
PRF1
GZMB
IFNG
TNF
CXCR5
BCL6
CD40LG
PD1
CTLA4
FOXP3
IL2RA
B Cells
CD19
CD27
BCL6
AID
IGHD
IGHG1
IGKC
Plasma Cells
JChain
IGKC
CD19
SDC1
PRDM1
Low
Hi
Normalized Log2
D
Pt-19
1
2
3
600 um
1
2
3
600 um

530

Fig.1. Identification of active T and B cell responses in PDAC by scRNA-Seq. (**A**) UMAP clusters are shown of immune cells isolated from six primary PDAC. (**B**) The cell numbers of different immune cell types identified in individual patient are shown. (**C**) The expression of selected genes in T cell, B cell and PC clusters are shown. The intensity of the colors represents the normalized log2 transformation of UMI. (**D**) Examples of TLS like structures (indicated by arrowhead and labelled with 1,2 and 3) in patient-19. The zoom in examples of TLS were shown in the right. Scale bar represents 600um.

Figure 2.

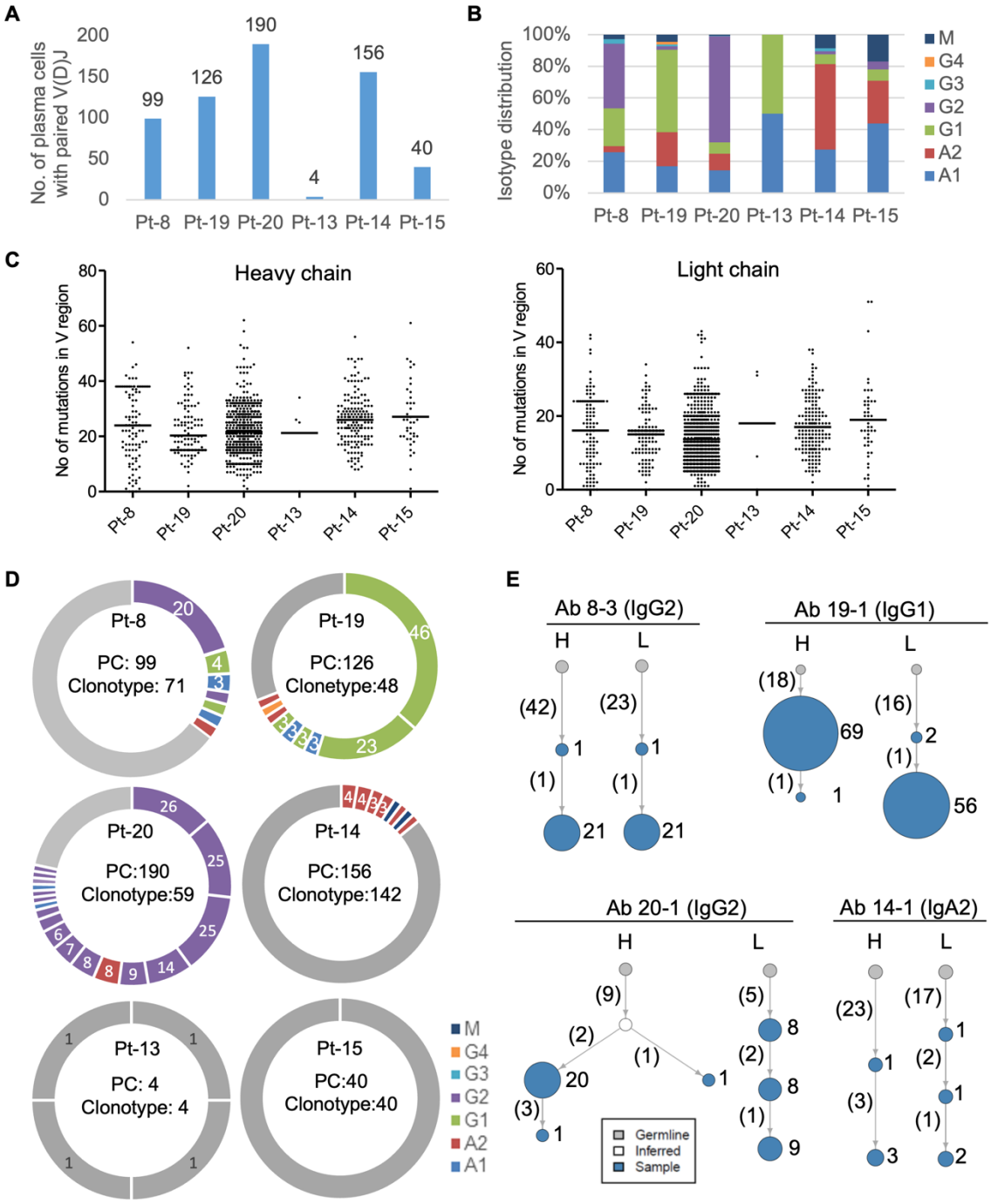
A
No. of plasma cells with paired V(D)J
200
150
100
50
0
99
126
190
4
156
40
Pt-8 Pt-19 Pt-20 Pt-13 Pt-14 Pt-15
B
Isotype distribution
100%
80%
60%
40%
20%
0%
Pt-8 Pt-19 Pt-20 Pt-13 Pt-14 Pt-15
M
G4
G3
G2
G1
A2
A1
C
Heavy chain
No of mutations in V region
Pt-8 Pt-19 Pt-20 Pt-13 Pt-14 Pt-15
Light chain
No of mutations in V region
Pt-8 Pt-19 Pt-20 Pt-13 Pt-14 Pt-15
D
Pt-8
PC: 99
Clonotype: 71
Pt-19
PC:126
Clonetype:48
Pt-20
PC:190
Clonotype:59
Pt-14
PC:156
Clonotype:142
Pt-13
PC: 4
Clonotype: 4
Pt-15
PC:40
Clonotype:40
M
G4
G3
G2
G1
A2
A1
E
Ab 8-3 (IgG2)
Ab 19-1 (IgG1)
Ab 20-1 (IgG2)
Ab 14-1 (IgA2)
H
L
Germline
Inferred
Sample

Fig.2. Identification of isotype switched and somatically hypermutated Igs by sequencing of PCs from PDAC. (**A**) Numbers are shown of PCs in which paired H and L chains were sequenced in each patient. The distribution of Ig isotypes (**B**) and the number of somatic mutations in V regions (**C**) in PCs from individual patients are determined. (**D**) The PCs with paired H and L chains and their clonotype distribution are shown for each patient. PCs within expanded clones are labelled with colored doughnuts, with colors indicating isotypes. Each slice represents one clone, with clone size proportional to slice size. Single clone PCs are pooled and labeled with gray color. (**E**) Examples are presented of antibody lineage evolution within expanded PC clones for individual patients. Clone size is indicated by the size of the node (not scaled) and labeled by numbers on the right. The number of somatic mutations in the combined V(D)J regions is shown in parenthesis.

Figure 3.

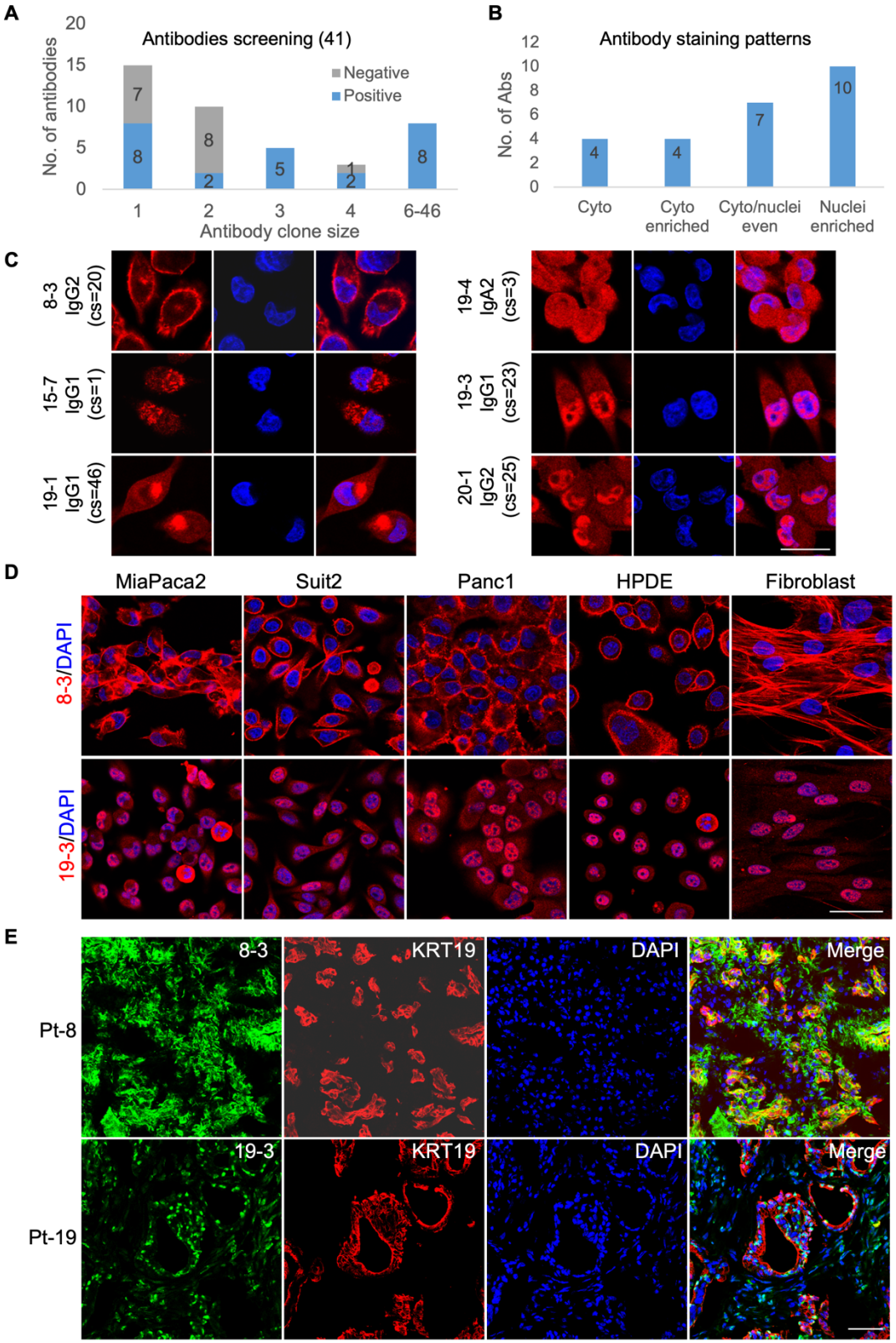
A
Antibodies screening (41)
No. of antibodies
Negative
Positive
Antibody clone size
1
2
3
4
6-46
B
Antibody staining patterns
No. of Abs
Cyto
Cyto enriched
Cyto/nuclei even
Nuclei enriched
C
8-3 IgG2 (cs=20)
15-7 IgG1 (cs=1)
19-1 IgG1 (cs=46)
19-4 IgA2 (cs=3)
19-3 IgG1 (cs=23)
20-1 IgG2 (cs=25)
D
MiaPaca2
Suit2
Panc1
HPDE
Fibroblast
8-3/DAPI
19-3/DAPI
E
Pt-8
Pt-19
8-3
19-3
KRT19
DAPI
Merge

596 **Fig.3. Recognition of intracellular self-antigens by recombinant antibodies from expanded PCs of**
597 **PDAC tumors.** (**A**) Summary is presented of the results of staining various cell lines by 41 recombinant
598 antibodies based on scRNA-Seq of PCs and B cells from six PDAC tumors, distributed according to clone
599 sizes. (**B-C**) The distribution and examples are shown of four distinct antibody staining patterns:
600 cytoplasmic (Cyto, e.g. 8-3 and 15-7), cytoplasmic enriched (Cyto enriched. e.g. 19-1), evenly distributed
601 in cytoplasmic and nuclei (Cyto/nuclei even, e.g. 19-1), and nuclei enriched (e.g. 19-3 and 20-1).
602 Examples of positive antibody staining (red) in MiaPaca2 cell line, co-stained with DAPI (blue). Original
603 antibody isotype and clone size (cs) are indicated. (**D**) The recombinant antibodies, 8-3 and 19-3 (red),
604 respectively, were used for staining different PDAC and non-cancer cell lines, along with nuclear staining
605 with DAPI (blue). (**E**) Antibodies 8-3 and 19-3, respectively, were used to stain the PDAC tumors from
606 which their PCs were derived. Staining was also done with anti-KRT19 antibody to demonstrate the
607 cancer cells. Scale bar in C, 25um, and in D and E, 50um.

Figure 4.

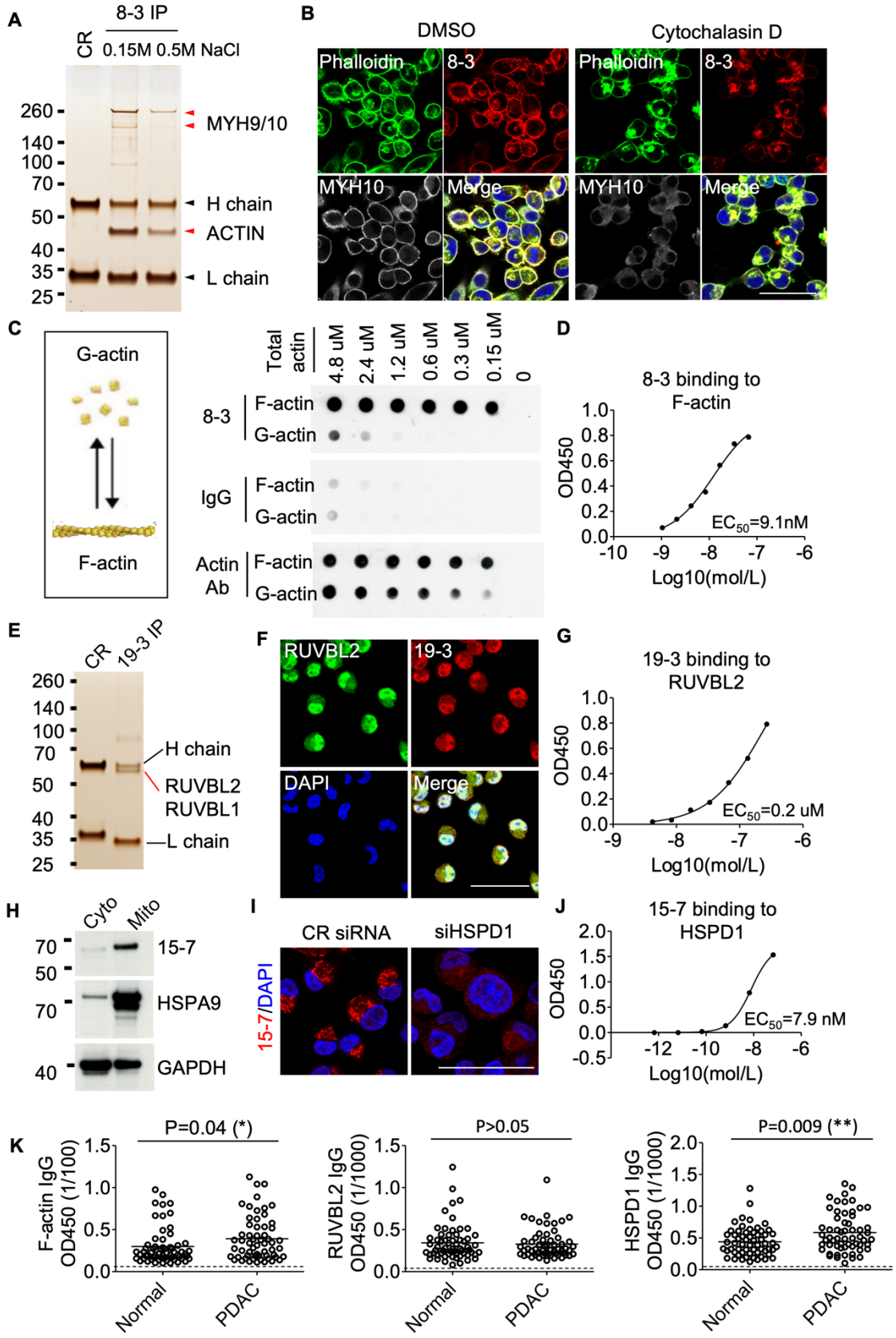
A
8-3 IP
CR
0.15M 0.5M NaCl
260
140
100
70
50
40
35
25
MYH9/10
H chain
ACTIN
L chain
B
DMSO
Cytochalasin D
Phalloidin
8-3
MYH10
Merge
C
G-actin
F-actin
Total actin
4.8 uM
2.4 uM
1.2 uM
0.6 uM
0.3 uM
0.15 uM
0
8-3
IgG
Actin Ab
F-actin
G-actin
D
8-3 binding to F-actin
OD450
EC50=9.1nM
Log10(mol/L)
E
CR
19-3 IP
H chain
RUVBL2
RUVBL1
L chain
F
RUVBL2
19-3
DAPI
Merge
G
19-3 binding to RUVBL2
EC50=0.2 uM
H
Cyto
Mito
15-7
HSPA9
GAPDH
I
CR siRNA
siHSPD1
15-7/DAPI
J
15-7 binding to HSPD1
EC50=7.9 nM
K
P=0.04 (*)
F-actin IgG OD450 (1/100)
P>0.05
RUVBL2 IgG OD450 (1/1000)
P=0.009 (**)
HSPD1 IgG OD450 (1/1000)
Normal
PDAC

609 **Fig.4. Identification of F-actin, RUVBL2 and HSPD1 as antigens in PDAC.** (**A**)
610 Proteins that were immunoprecipitated by antibody 8-3 from lysates of MiaPaca2 cells were
611 separated by SDS-PAGE and visualized by silver staining. Two bands were identified by
612 mass spectrometry (red arrowheads). (**B**) MiaPaca2 cells were co-stained with 8-3,
613 phalloidin, and an antibody specific for MYH10 after 30min treatment of the cells with
614 DMSO or cytochalasin D. (**C**) Dot-blot assay is shown the reaction with F-actin or G-actin
615 of 8-3, isotype control IgG, and a commercial actin specific antibody. (**D**) The binding of
616 incremental concentrations of 8-3 to F-actin was measured by ELISA. (**E**) Proteins that
617 were immunoprecipitated by recombinant antibody 19-3 from lysates of MiaPaca2 cells
618 were separated by SDS-PAGE and visualized by silver staining. The proteins, RUVBL1
619 and RUVBL2, were identified by mass spectrometry. (**F**) MiaPaca2 cell were co-stained
620 with 19-3 and an antibody specific for RUVBL2. (**G**) The binding of incremental
621 concentrations of 19-3 to RUVBL2 was measured by ELISA. (**H**) Western blot analysis of
622 recombinant antibody 15-7 detection of cytoplasmic proteins (Cyto) and mitochondria-
623 enriched proteins (Mito) is shown. (**I**) Immunofluorescent staining of MiaPaca2 cells by 15-
624 7 and an antibody specific for HSPD1 is shown. (**J**) The binding of incremental
625 concentrations of 15-7 to HSPD1 was measured by ELISA. (**K**) The serum IgG titers of
626 normal individuals and PDAC patients to F-actin (sera diluted 1:100), to RUVBL2 (sera
627 diluted 1:1000), and to HSPD1(sera diluted 1:1000), respectively, were measured by
628 ELISA. The non-parametric t-test was used for comparison. Scale bars in **B**, **F** and **I** are
629 50um.
630
631
632

633 **Title: Plasma cells in human pancreatic ductal adenocarcinoma secrete antibodies to self-**

634 **antigens**

635 **Authors:** Min Yao[1]†, Jonathan Preall[1], Johannes Yeh[1], Darryl Pappin[1], Paolo Cifani[1], Yixin Zhao[1],

636 Sophia Shen[2], Philip Moresco[1,3,4], Brian He[1], Hardik Patel[1], Amber Habowski [1], Daniel A. King[5], Kara

637 Raphael[5], Arvind Rishi[5], Divyesh Sejpal[5]‡, Matthew Weiss[5], David Tuveson[1], Douglas Fearon[1,6*]

638

639 **Supplementary materials**

640 **Supplementary figures**

641

642

Supplementary figure 1.

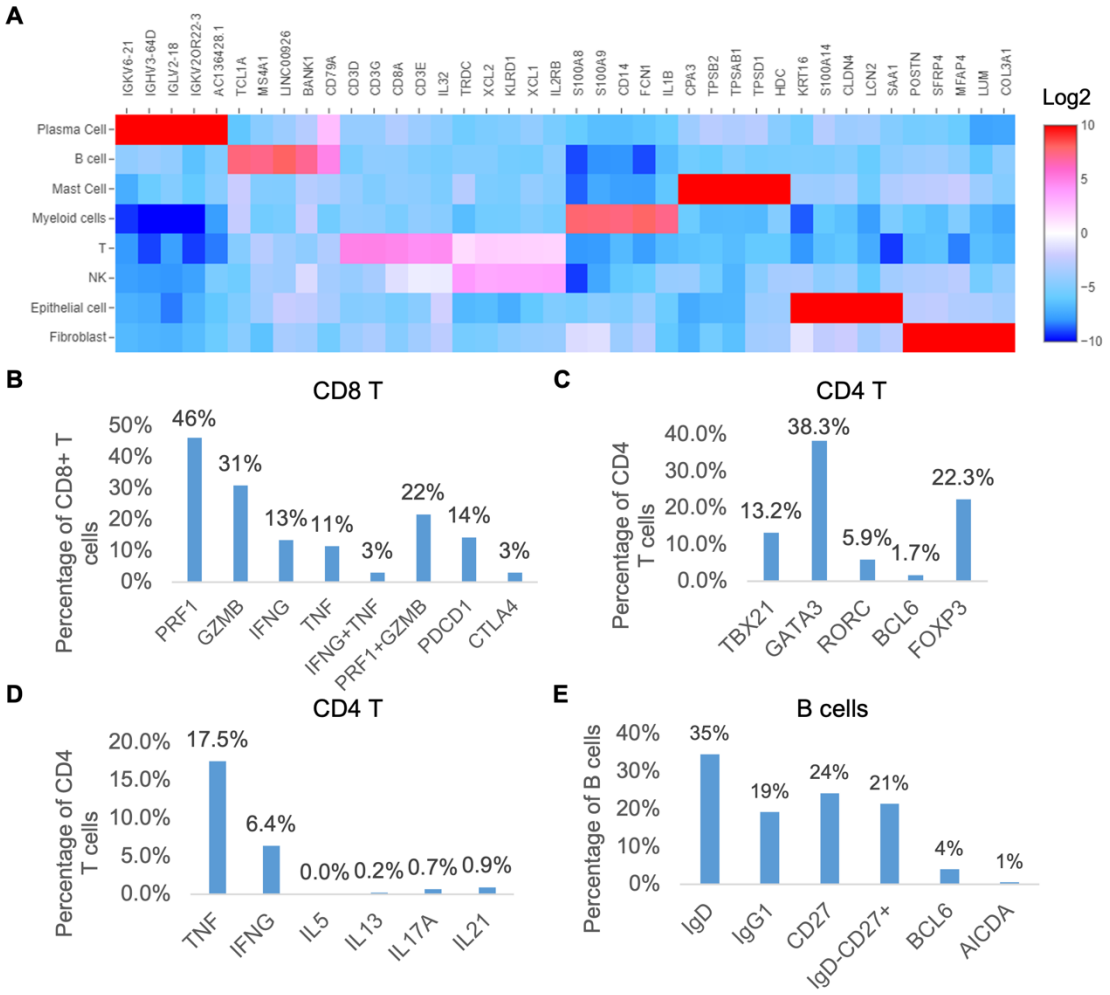

Fig. S1. Characterization of primary PDAC immune cells microenvironment by scRNA-Seq. (A) Heatmap of the top five most upgraded genes in each cell cluster defined in Figure 1A. Color scale is log2 fold changes. (**B-E**) The percentage of cells expressing selected gene markers in the clusters of CD8 T (**B**), CD4 (**C, D**) and B cells (**E**).

Supplementary figure 2.

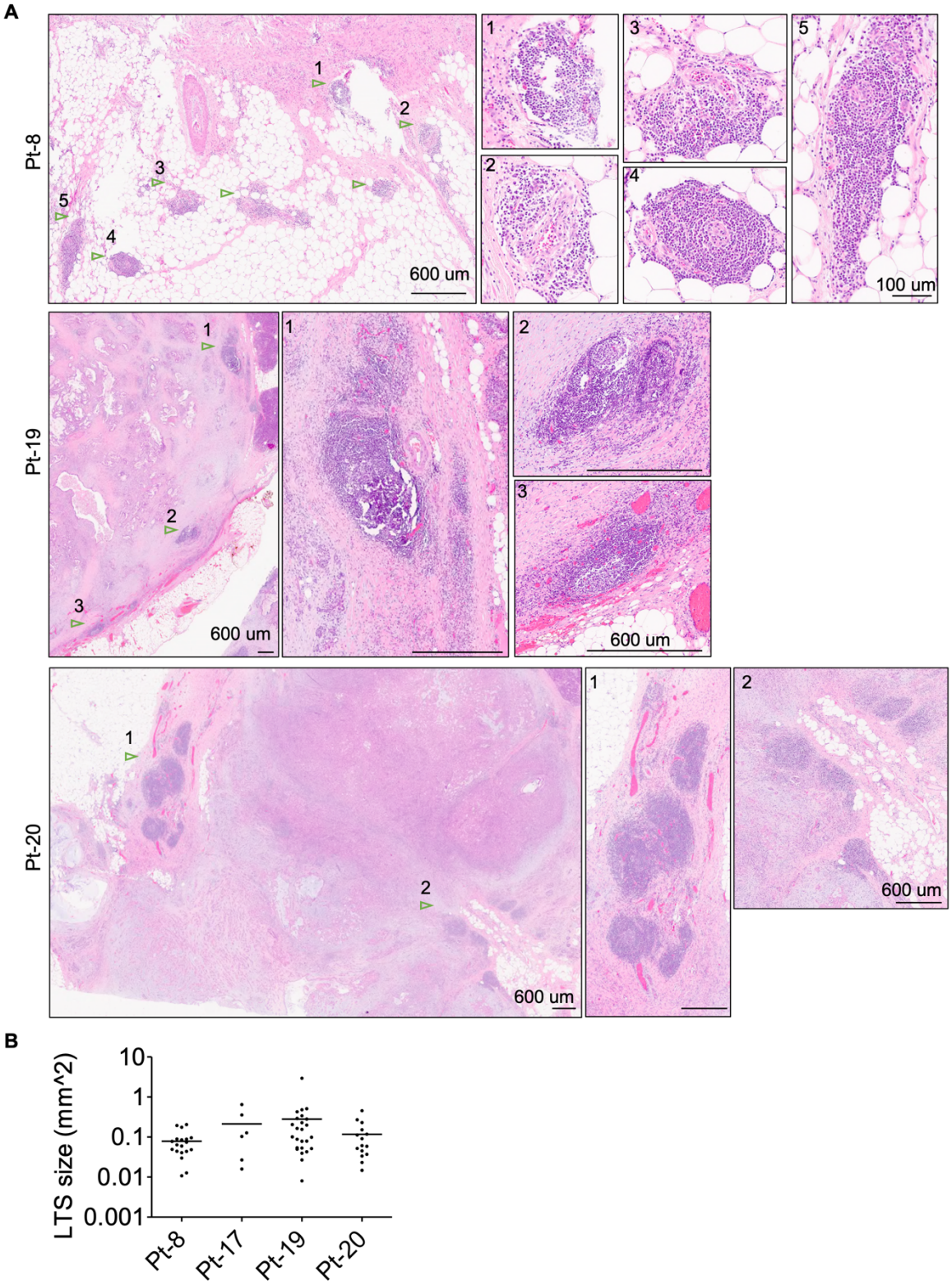

654 **Fig. S2. Presence of TLS like structures in PDAC. (A)** Examples of TLS like structures in patient 8, 19
655 and 20 (TLS indicated by arrowhead and labelled by numbers). The zoom in images were shown in the
656 right. Scale bar is shown in figures. (**B**) Quantification and size distribution of the TLS in the four
657 resected PDAC samples. Only TLS with size bigger than 0.01 mm^2 were analyzed.
658

Supplementary figure 3.

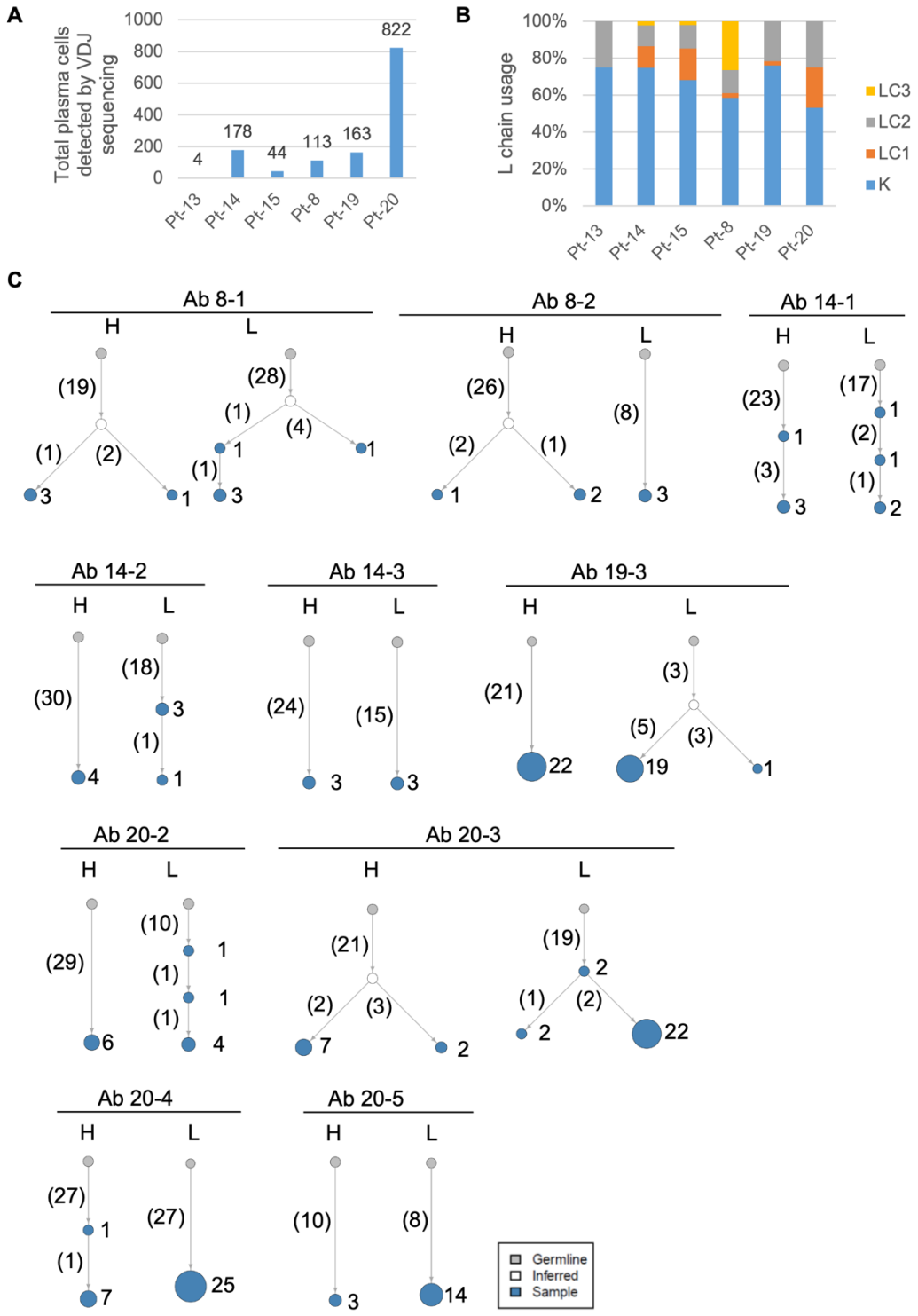

660 **Fig. S3. Additional Ig sequences evolution trees from PCs in PDAC.** Additional examples of antibody
661 lineage evolution among top expanded PC clones screened in this study. Clone size is indicated by the
662 size of the node (not scaled) and labeled by numbers on the right. The clone size includes both paired and
663 unpaired chains. Number of somatic mutations in combined V(D)J regions is shown in parenthesis.
664
665
666
667

Supplementary figure 4.

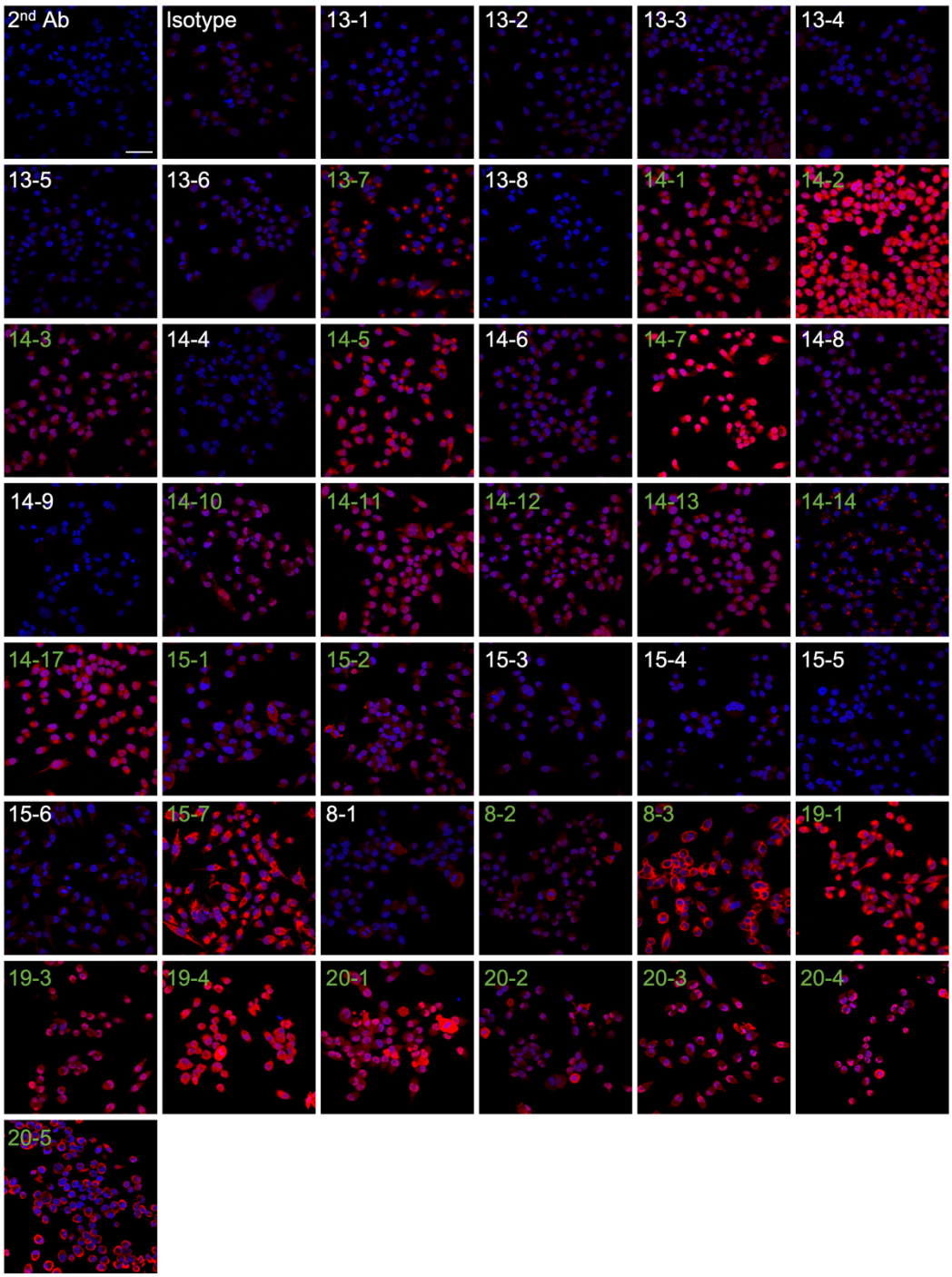

Fig. S4. Antibodies staining atlas on MiaPaca2 cell line. MiaPaca2 cells were stained with each antibody (red) and co-stained with DAPI (blue). Secondary antibody only (2nd Ab) and isotype IgG were used as control. Antibodies with positive staining are labeled green, and antibodies with negative staining

672 are labeled white. All images were acquired using the same confocal setting for isotype control staining,

673 and the gain on the query antibody was reduced if the images were saturated. Scale bar is 50um.

Supplementary figure 5.

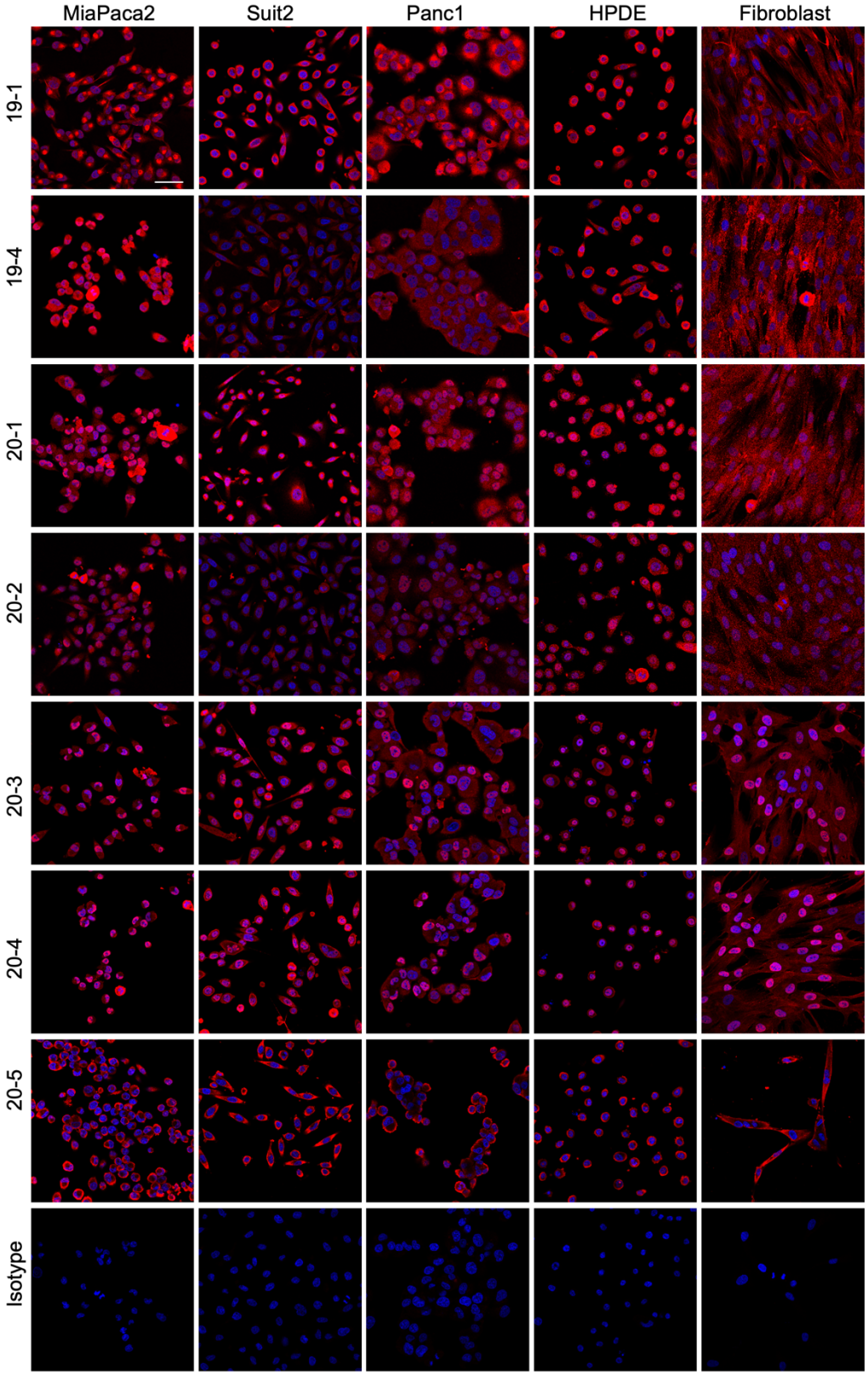

675 **Fig. S5. Examples of antibodies staining in PDAC and non-cancer cell lines.** Cells were stained with

676 each antibody (red) and co-stained with DAPI (blue). Scale bar is 50um.

Supplementary figure 6.

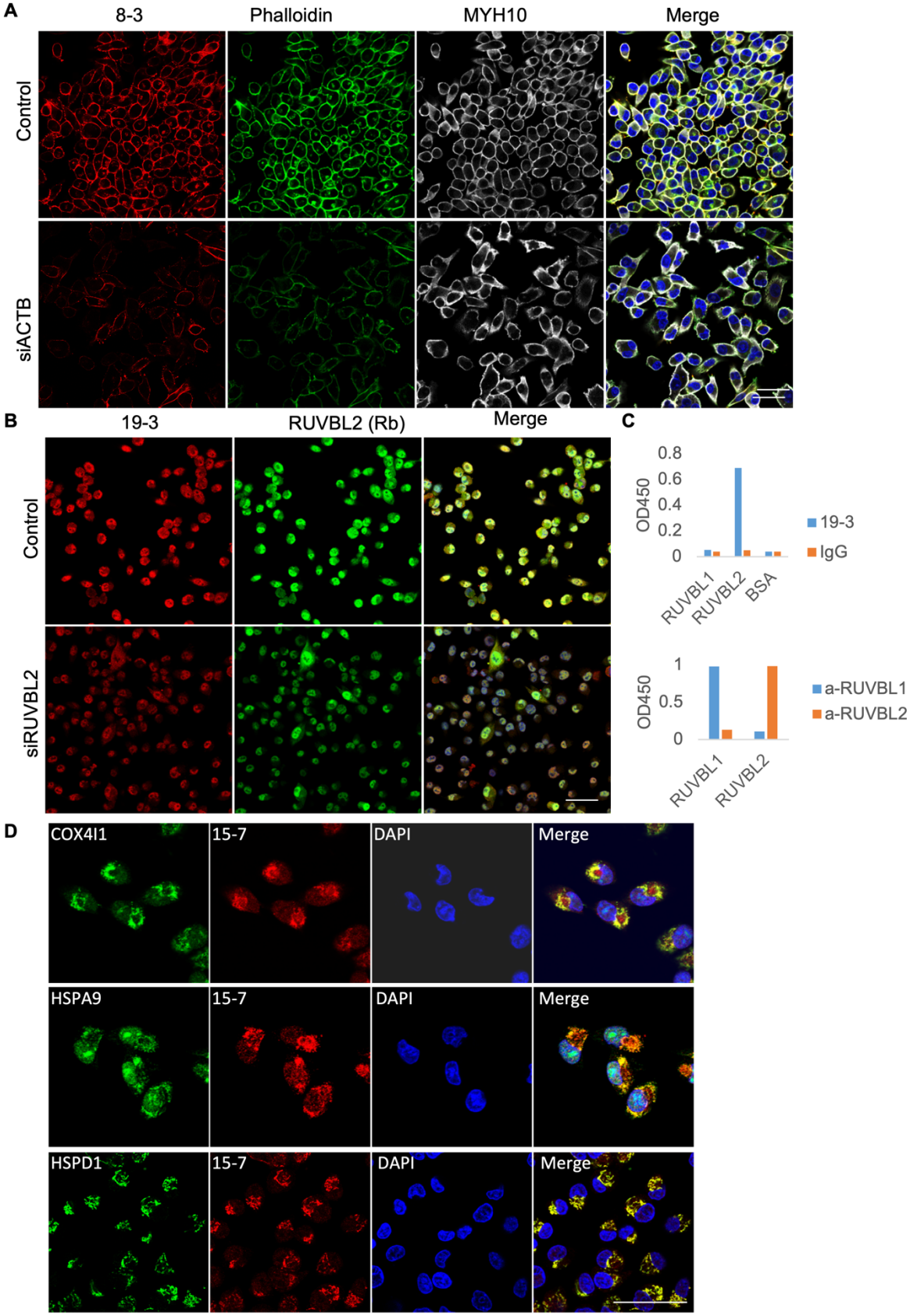

677

678 **Fig. S6. Characterization of antibodies 8-3, 19-3 and 15-7.** (**A**) 8-3 staining after siRNA knockdown of
679 *ACTB* in MiaPaca2 cells, co-stained with phalloidin, MYH10 antibody and DAPI. (**B**) Measurement of
680 19-3 binding to recombinant RUVBL1 and RUBL2 proteins by ELISA. Positive controls using
681 polyclonal rabbit antibodies anti-RUVBL1 (a-RUVBL1) or anti-RUVBL2 (a-RUVBL2). (**C**) 19-3
682 staining after siRNA knockdown of *RUVBL2* in MiaPaca2 cells, co-stained with anti-RUVBL2 rabbit
683 antibody and DAPI. (**D**) Co-staining of 15-7 with mitochondria markers COX4I1, HSPA9 and HSPD1 in
684 MiaPaca2 cells. Scale bars in A, C and D are 50um.
685
686
687
688
689
690
691

Supplementary figure 7.

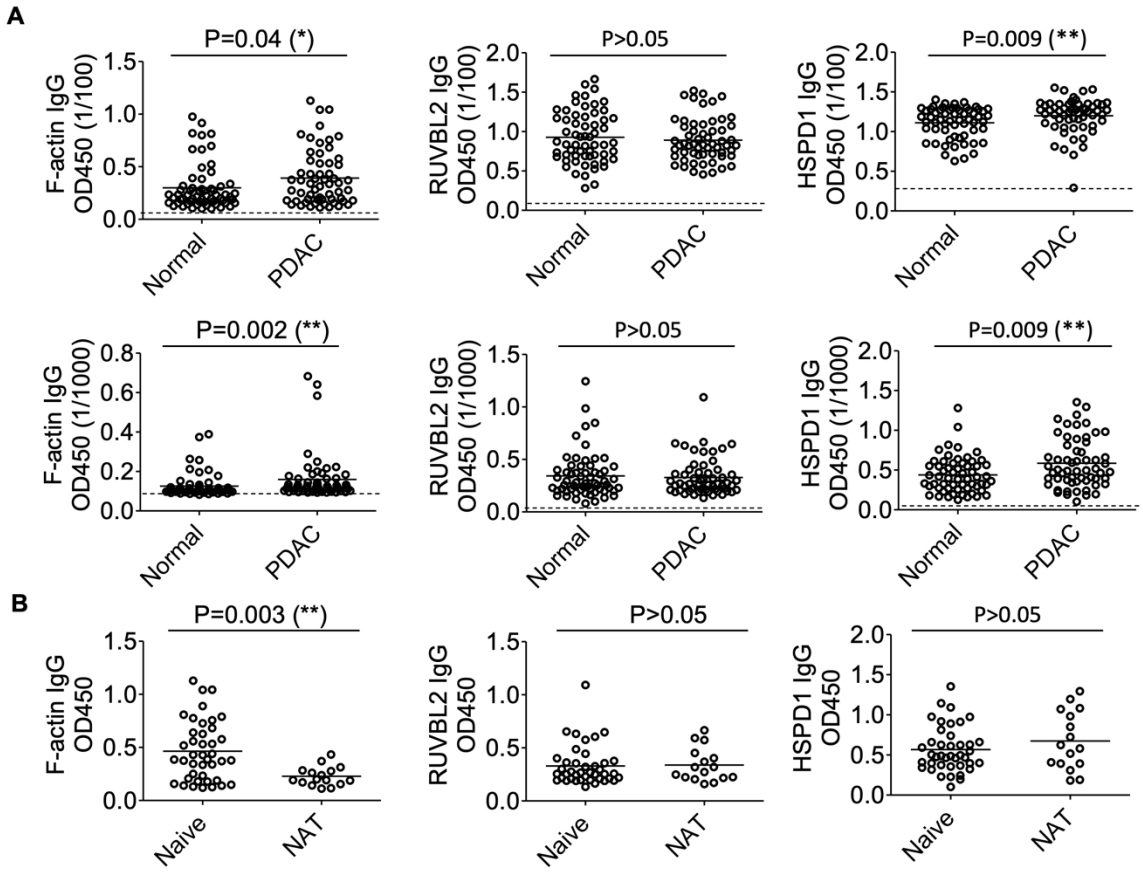

692

693 **Fig. S7. Comparison of plasma IgG titers to F-actin, RUVBL2 and HSPD1 between healthy donors**
694 **and PDAC patients.** (**A**) Comparison of IgG titer to F-actin, RUVBL2 and HSPD1 of plasma samples
695 diluted at 1/100 or 1/1000 by ELISA. Background signals from secondary antibody only are shown in a
696 dashed line. (**B**) Comparison of IgG response to F-actin, RUVBL2 and HSPD1 between naïve treated
697 (naive) and neoadjuvant treated (NAT) PDAC patients. The non-parametric t-test is used for comparisons.

698

699

700

701

702

703

704 **Table S1. Human PDAC samples information for scRNA-Seq studies.**

Patient ID	Pt-8	Pt-17	Pt-19	Pt-20	Pt-13	Pt-14	Pt-15
Diagnosis	PDAC	PDAC	PDAC	PDAC	PDAC	PDAC	PDAC
Collection method	resection	resection	resection	resection	FNA	FNA	FNA
Age	58	75	71	67	40	89	53
Gender	Male	Male	Female	Female	Female	Male	Female
Race	Caucasian	Caucasian	African-American	Asian	Latino/Hispanic	Caucasian	African American
Neoadjuvant therapy	No	No	No	No	No	No	No
TNM stage	pT2N2Mx	pT2N1Mx	pT2N1	pT2N0	NA	NA	NA
Tumor size (cm)	2.2*1.5*1	2.7*2.6*2.5	2.7*2.3*2.2	2.2*1.7*0.8	NA	NA	NA
MSI status	MSS	MSS	MSS	MSS	NA	NA	NA
Tumor organoid available	Yes	No	No	Yes	Yes	Yes	No
Tumor section available	Yes	Yes	Yes	Yes	No	No	No
Gene Expressing Sequencing	Yes	Yes	Yes	Yes	Yes	Yes	Failed
Ig sequencing	Yes	Yes (low B and PC cells)	Yes	Yes	Yes	Yes	Yes

705 Abbreviations: FNA, fine needle aspiration; MSI, microsatellite instable; MSS, microsatellite stable; NA,

706 not available/appliable

707

708

709 **Table S2. List of antibodies synthesized and screening results.**

No	Patient	Ab-name	Clone size	Cell type	Isotype	Light chain	Binding reactivity	Antigen location	Antigen identity	Synthesize format
1	Pt-8	8-1	4	PC	IgG1	IgK	Negative	NA		IgG4-His
2	Pt-8	8-2	3	PC	IgA1	IgK	Positive	nuclei enriched	Unknown	IgG4-His
3	Pt-8	8-3	20	PC	IgG2	IgLC3	Positive	cyto	F-actin	IgG4-His
4	Pt-19	19-1	46	PC	IgG1	IgK	Positive	cyto enriched	Unknown	IgG4-His
5	Pt-19	19-3	23	PC	IgG1	IgK	Positive	nuclei enriched	RUVBL2	IgG4-His
6	Pt-19	19-4	3	PC	IgA2	IgK	Positive	cyto/nuclei even	Unknown	IgG4-His
7	Pt-20	20-1	25	PC	IgG2	IgLC2	positive	nuclei enriched	Unknown	IgG4-His
8	Pt-20	20-2	6	PC	IgG2	IgLC1	positive	nuclei enriched	Unknown	IgG4-His
9	Pt-20	20-3	26	PC	IgG2	IgLC1	positive	nuclei enriched	Unknown	IgG4-His
10	Pt-20	20-4	25	PC	IgG2	IgK	positive	nuclei enriched	Unknown	IgG4-His
11	Pt-20	20-5	14	PC	IgG2	IgK	positive	cyto	Unknown	IgG4-His
12	Pt-13	13-1	1	PC	IgG1	IgK	Negative	NA		IgG1
13	Pt-13	13-2	1	PC	IgG1	IgLC2	Negative	NA		IgG1
14	Pt-13	13-3	1	PC	IgA1	IgK	Negative	NA		IgG1
15	Pt-13	13-4	1	PC	IgG1	IgK	Negative	NA		IgG1
16	Pt-13	13-5	1	PC	IgA1	IgK	Negative	NA		IgG1
17	Pt-13	13-6	1	GC-B	IgG1	IgK	Negative	NA		IgG1
18	Pt-13	13-7	1	GC-B	IgG3	IgLC2	Positive	cyto	Unknown	IgG1
19	Pt-13	13-8	2	B	IgA1	IgLC2	Negative	NA		IgG1
20	Pt-14	14-1	4	PC	IgA2	IgK	Positive	cyto/nuclei even	Unknown	IgG1
21	Pt-14	14-2	4	PC	IgA2	IgK	Positive	cyto/nuclei even	Unknown	IgG1
22	Pt-14	14-3	3	PC	IgA2	IgK	Positive	nuclei enriched	Unknown	IgG1
23	Pt-14	14-4	2	PC	IgM	IgK	Negative	NA		IgG1
24	Pt-14	14-5	2	PC	IgA1	IgK	Positive	cyto enriched	Unknown	IgG1
25	Pt-14	14-6	2	PC	IgA2	IgK	Negative	NA		IgG1
26	Pt-14	14-7	2	PC	IgA2	IgK	Positive	nuclei enriched	Unknown	IgG1
27	Pt-14	14-8	2	PC	IgA2	IgLC3	Negative	NA		IgG1
28	Pt-14	14-9	1	PC	IgM	IgK	Negative	NA		IgG1
29	Pt-14	14-10	1	PC	IgM	IgLC2	Positive	nuclei enriched	Unknown	IgG1
30	Pt-14	14-11	1	PC	IgA2	IgLC1	Positive	nuclei enriched	Unknown	IgG1
31	Pt-14	14-12	1	PC	IgG1	IgK	Positive	nuclei enriched	Unknown	IgG1

32	Pt-14	14-13	1	PC	IgA2	IgK	Positive	cyto/nuclei even	Unknown	IgG1
33	Pt-14	14-14	1	PC	IgA2	IgK	Positive	cyto	Unknown	IgG1
34	Pt-14	14-17	1	PC	IgG3	IgK	Positve	cyto enriched	Unknown	IgG1
35	Pt-15	15-1	3	B	IgA2	IgK	Positive	cyto/nuclei even	Unknown	IgG1
36	Pt-15	15-2	3	B	IgA1	IgK	Positive	cyto/nuclei even	Unknown	IgG1
37	Pt-15	15-3	2	PC	IgM	IgKC	Negative	NA		IgG1
38	Pt-15	15-4	2	PC	IgA1	IgK	Negative	NA		IgG1
39	Pt-15	15-5	2	PC	IgA2	IgK	Negative	NA		IgG1
40	Pt-15	15-6	2	B	IgA2	IgLC1	Negative	NA		IgG1
41	Pt-15	15-7	1	PC	IgG1	IgK	Positive	cyto	HSPD1	IgG1

Abbreviations: PC-plasma cells, B- B cells, GC-B: Germinal center B cells, cyto-cytoplasmic

Light orange color indicates the three antibodies that have antigens identified.

729 **Table S3. Human samples information for plasma studies.**

		Normal (n=61)		PDAC (n=59)		Comparison
		No.	Ratio	No.	Ratio	p value
Gender	Male	22	36%	22	37%	n.s.
	Female	39	64%	32	54%	
	Unknown	0	0%	5	8%	
Age	Median (range)	36	17-66	69.5	49-89	<0.0001
	Unknown	0		5		
Race	Asian	7	11%	5	8%	<0.001
	African American	13	21%	7	12%	
	Caucasian	8	13%	40	68%	
	Hispanic	33	54%	2	3%	
	NA	0	0%	5	8%	
Treatment	Neoadjuvant	-		16	27%	
	No pre-treatment	-		41	69%	
	NA	-		2	3%	
T stage	T1	-		4	7%	
	T2	-		26	44%	
	T3	-		13	22%	
	T4	-		1	2%	
	NA	-		15	25%	
N stage	N0	-		15	25%	
	N1	-		17	29%	
	N2	-		12	20%	
	NA	-		15	25%	
M stage	Mx	-		54	92%	
	M1	-		5	8%	

730

731

732

733

734

735

736

737

738